SOURCE DATA    TRANSPARENT PROCESS    OPEN ACCESS

THE EMBO JOURNAL

# Function of HNRNPC in breast cancer cells by controlling the dsRNA-induced interferon response

Yusheng Wu[1,2,3,4,†], Wenwei Zhao[2,3,4,†], Yang Liu[2,3,4,5,†], Xiangtian Tan[2,3,4], Xin Li[2,3,4], Qin Zou[2,3,4,5], Zhengtao Xiao[1,2,3,4], Hui Xu[1,2,3,4], Yuting Wang[2,3,4,5] & Xuerui Yang[1,2,3,4,*] (iD)

## Abstract

Elevated expression of RNA binding protein HNRNPC has been reported in cancer cells, while the essentialness and functions of HNRNPC in tumors were not clear. We showed that repression of HNRNPC in the breast cancer cells MCF7 and T47D inhibited cell proliferation and tumor growth. Our computational inference of the key pathways and extensive experimental investigations revealed that the cascade of interferon responses mediated by RIG-I was responsible for such tumor-inhibitory effect. Interestingly, repression of HNRNPC resulted in accumulation of endogenous double-stranded RNA (dsRNA), the binding ligand of RIG-I. These up-regulated dsRNA species were highly enriched by Alu sequences and mostly originated from pre-mRNA introns that harbor the known HNRNPC binding sites. Such source of dsRNA is different than the recently well-characterized endogenous retroviruses that encode dsRNA. In summary, essentialness of HNRNPC in the breast cancer cells was attributed to its function in controlling the endogenous dsRNA and the down-stream interferon response. This is a novel extension from the previous understandings about HNRNPC in binding with introns and regulating RNA splicing.

## Introduction

Aberrant up-regulation of heterogeneous nuclear ribonucleoprotein C (HNRNPC) has been observed in multiple tumors or tumor cell lines, including glioblastoma (Park et al, 2012), hepatocellular carcinoma (Sun et al, 2007), melanoma (Mulnix et al, 2014), and lung cancer (Pino et al, 2003). As an RNA binding protein (RBP), HNRNPC is well known for its regulatory roles in RNA splicing (Konig et al, 2010; Zarnack et al, 2013), sequence-unspecific RNA exportation (McCloskey et al, 2012), RNA expression (Christian et al, 2008; Park et al, 2012), stability (Shetty, 2005; Velusamy et al, 2008), 3′ end processing (Gruber et al, 2016), and translation (Kim et al, 2003; Meng et al, 2008; Spahn et al, 2008; Lee et al, 2010). Indeed, among these HNRNPC-involved regulatory events are processing of multiple cancer-related genes, including BRCA (Anantha et al, 2013), uPAR (Shetty, 2005), MALAT1 (Yang et al, 2013), PDCD4 (Park et al, 2012), cMyc (Kim et al, 2003). However, the essentialness of HNRNPC in tumors and the exact molecular processes that are responsible for the potential physiological function of HNRNPC in the tumor cells are still not clear. In the present study, we showed that even a partial repression of HNRNPC could result in arrestment of cell proliferation and tumorigenesis of the breast cancer cell lines MCF7 and T47D, suggesting an indispensable role of HNRNPC in these cells. Our further survey of the transcriptome profiles after HNRNPC knock-down in these cells revealed an unanticipated dramatic elevation of the interferon-stimulated genes (ISGs), including the type I interferon IFNβ itself.

IFNβ can be expressed in most of the cell types upon invasion of microbes and sensing of the microbial components by the pattern recognition receptors (PRRs; Nagarajan, 2011; Schneider et al, 2014). In addition, the type I interferon production can also be activated by the PRRs sensing the endogenous nucleic acids under stress conditions such as radiation, autoimmune disease, and cancer (West et al, 2015; Roers et al, 2016). Specifically, upon activation by their ligands, the cytoplasmic DNA sensors (ALR and cGAS) and RNA sensors (RIG-I and MDA5) initiate the signaling cascade of interferon response (Honda et al, 2006; Goubau et al, 2013; Wu & Chen, 2014; McNab et al, 2015), leading to transcription of the ISGs (Platanias, 2005; Schneider et al, 2014). These interferon responses have been shown to be involved in regulating tumor development due to its well-characterized pro-apoptotic and anti-proliferative effects in various types of cancer cells, including myeloma cell lines (Chen et al, 2001), lymphoma (Yang et al, 2012), liver cancer cells (Maeda et al, 2014; Murata et al, 2006; Sangfelt et al, 1997), and

sarcoma cell lines (Sanceau *et al*, 2000). In fact, recent studies have shown that the IFN response triggered by endogenous dsRNA plays a central role in executing the therapeutic effects of anti-tumor drugs such as DNA methyltransferase inhibitors and CDK4/6 inhibitors in multiple types of cancer (Chiappinelli *et al*, 2015; Roulois *et al*, 2015; Goel *et al*, 2017).

In the present study, we showed that the tumor-inhibitory effect of HNRNPC knock-down was mediated through the cascade of interferon response, which was specifically initiated via retinoic acid-inducible gene I (RIG-I, gene name DDX58), but not the other PRRs. Interestingly, we found that HNRNPC knock-down resulted in increase in the endogenous double-stranded RNA (dsRNA), which is the binding ligand of RIG-I. We then developed a dsRNA pull-down-based experiment to enrich the dsRNA species from the total RNA. Sequencing of these dsRNA libraries and the following bioinformatics analysis systematically identified the dsRNA regions and quantified their abundances. Accumulation of some dsRNA regions was indeed observed after HNRNPC knock-down. These elevated dsRNA species were mostly found in introns, corroborating known transcriptome-wide HNRNPC binding regions (Konig *et al*, 2010; Zarnack *et al*, 2013). This differs from previous observation of elevated dsRNA derived from normally hypermethylated endogenous retroviruses (ERVs) that are activated by anti-tumor inhibitors to trigger the IFN response as a therapeutic approach (Chiappinelli *et al*, 2015; Roulois *et al*, 2015; Goel *et al*, 2017). Heterogeneous nuclear ribonucleoprotein C is well known for its function in regulating RNA splicing by binding with introns, especially the introns containing Alu (Konig *et al*, 2010; Zarnack *et al*, 2013). Indeed, almost all the up-regulated dsRNA regions contain Alu or Alu fragments. Therefore, our discovery of dsRNA accumulation upon HNRNPC repression is a novel extension of the previously characterized functions of HNRNPC in binding with pre-mRNA introns and regulating RNA splicing.

# Results

## Repression of HNRNPC arrested the proliferation and tumorigenesis of MCF7 and T47D

Elevated expression of HNRNPC has been observed in multiple types of tumors and tumor cells (Pino *et al*, 2003; Sun *et al*, 2007; Park *et al*, 2012; Mulnix *et al*, 2014). The present study was focused on the potential function of HNRNPC in breast cancer cells. The RNA-seq data of breast cancer in The Cancer Genome Atlas (TCGA) also showed a significant increase in HNRNPC expression in 111 breast cancer tumors compared to their adjacent normal tissues (Appendix Fig S1). Gene expression knock-down of HNRNPC with siRNAs (Appendix Fig S2A–D) greatly reduced the proliferation rates of two breast cancer cell lines, MCF7 and T47D (Fig 1A and B, and Appendix Fig S3A and B). This was confirmed by CRISPR/Cas9-mediated partial knock-down of HNRNPC (Appendix Fig S4A and B), which suppressed cell proliferation as well ($P < 0.05$ for MCF7 and 0.01 for T47D, Fig 1C and D). The anchorage-independent growth assay further showed that shRNA-mediated silencing of HNRNPC (Appendix Fig S4C and D) strongly repressed colony formation of MCF7 and T47D (Fig 1E and F), indicating the reduced malignant transformation potential. However, such proliferation-inhibitory effect of HNRNPC repression is absent in the primary

breast epithelial cell MCF10A or in the triple-negative breast cancer cells BT549 and MDA-MB-231 (Appendix Fig S5A–F).

Consistently, xenograft transplantation mouse models demonstrated that shRNA-mediated long-term knock-down of HNRNPC (Appendix Fig S4E) greatly repressed the *in vivo* tumorigenesis of MCF7 (Fig 1G). Furthermore, periodic (half-weekly) injection of the HNRNPC siRNA packed with a polymer-based delivery reagent, into the MCF7 cell-derived xenograft tumors, also repressed tumor growth *in vivo* ($P < 0.01$, Fig 1H and Appendix Fig S4F). Taken together, these results suggest that HNRNPC is indispensable for the proliferation and tumorigenesis of the cells MCF7 and T47D.

## Repression of HNRNPC activated the type I interferon response

To further elucidate the molecular mechanism for the potent tumor-inhibitory function of HNRNPC repression in the breast cancer cells, we profiled the genome-wide gene expression levels with RNA-seq upon HNRNPC knock-down in MCF7 and T47D cells. Silencing of HNRNPC with siRNAs in MCF7 and T47D cells resulted in up-regulation of a number of genes (Fig 2A and B), which are highly and exclusively enriched by the genes involved in the interferon response-related processes, according to the gene ontology and KEGG pathway enrichment analyses (Fig 2C and D). Indeed, many of the up-regulated genes belong to the category of ISGs (Fig 2A and B). These results from RNA-seq were validated with qPCR experiments, which confirmed the elevated mRNA expressions of IFNβ (IFNB1) and multiple ISGs after HNRNPC knock-down (Fig 2E). Finally, this was further backed by the inducible CRISPR/Cas9-mediated silencing of HNRNPC, which also led to up-regulation of the ISGs (Fig 2F).

Next, we examined the differential activities of the transcription factors (TFs) that may have been driving the global gene expression profile shift in response to HNRNPC repression. Here, we used the MARINa (MAster Regulator INference algorithm), which were designed to identify the master TFs across two conditions by assessing the differential expression of the TF target gene sets (Lim *et al*, 2009). The MARINa analysis identified almost all the core TFs in the interferon response cascade (Fig 2G), including IRF3/7, the transcriptional activator of the IFNβ gene, and two components of the ISGF3 complex (STAT1 and IRF9), which is the down-stream TF effector of the interferon signaling pathway and responsible for the transcriptional up-regulation of the ISGs.

Taken together, these results indicate that suppression of HNRNPC in MCF7 and T47D resulted in both the first wave of interferon response, i.e., production of IFNβ potentially by transcription factors IRF3/7, and the second wave of interferon signaling pathway that activates the ISGF3 complex, leading to up-regulated expression of the ISGs. Indeed, high levels of IFNβ in the cell media were observed after HNRNPC knock-down (Fig 3A), and treatment of MCF7 and T47D cells with IFNβ induced up-regulation of the ISGs and inhibition of cell proliferation in a dose-dependent manner (Fig EV1A and B).

Interestingly, such a strong interferon response was absent in MCF10A, BT549, and MDA-MB-231 (Appendix Fig S6A–C), of which the proliferation rates were unaltered upon HNRNPC knock-down (Appendix Fig S5). This leads to the hypothesis that the production and secretion of IFNβ are responsible for the up-regulated ISGs in MCF7 and T47D, and the cascade of interferon production and signaling is responsible for the tumor-inhibitory effect of HNRNPC repression.
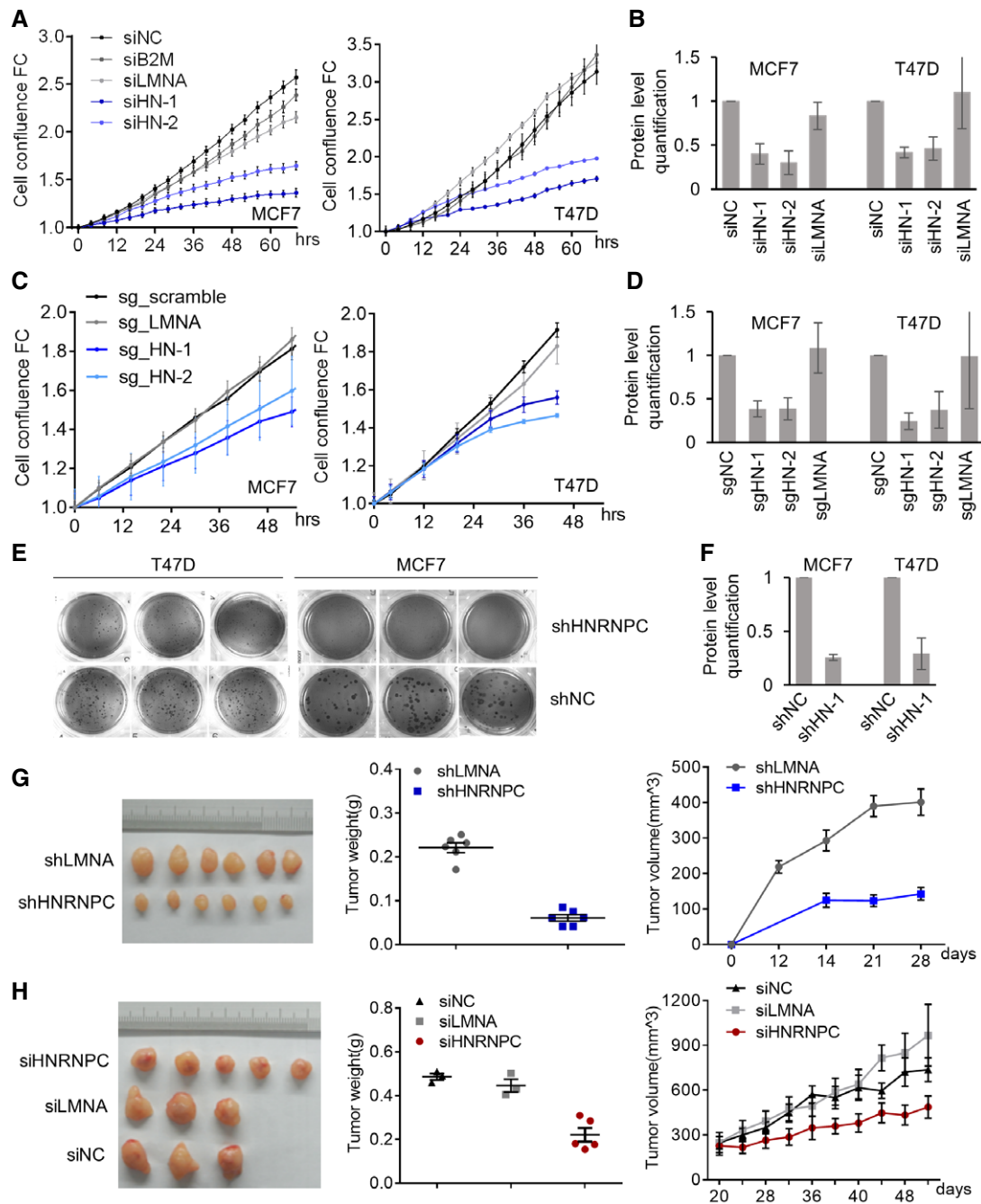
**Figure 1. Knock-down of HNRNPC inhibited growth and tumorigenesis of breast cancer cells.**

A   Growth curves of the MCF7 (left) and T47D cells (right) upon gene silencing with siRNAs. siNC: non-targeting siRNA as a negative control, siHN-1: siRNA sequence 1 for HNRNPC, siHN-2: siRNA sequence 2 for HNRNPC, siLMNA: siRNA for LMNA as another negative control. Each sample has three replicates. Data represent mean ± SD.

B   Relative protein levels of HNRNPC upon siRNA-mediated silencing, quantified from Western blots of three replicates. The error bars represent ± SD.

C   Growth curves of the Tet-on CRISPR-Cas9-MCF7 (left) and Tet-on CRISPR-Cas9-T47D cells (right). Expression of Cas9 was induced with 5 μM doxycycline after transfection of the sgRNAs. sgNC: non-targeting sgRNA as a negative control, sgHN-1: sgRNA sequence 1 for HNRNPC, sgHN-2: sgRNA sequence 2 for HNRNPC, sgLMNA: sgRNA for LMNA as another negative control. Each sample has three replicates. Data represent mean ± SD.

D   Relative protein levels of HNRNPC upon CRISPR-mediated gene knock-down, quantified from Western blots of three replicates. The error bars represent ± SD.

E   Anchorage-independent cell growth assays of the HNRNPC-deficient MCF7 (right) and T47D (left) cells.

F   Relative protein levels of HNRNPC upon shRNA-mediated silencing, quantified from Western blots of three replicates. The error bars represent ± SD.

G   Images, weights, and growth records of the xenograft tumor models in female NSG mice established from the MCF7 cells with lentivirus-mediated stable gene knock-down. Each group has six mice. The error bars represent ± SEM.

H   Images, weights, and growth records of the MCF7-derived xenograft tumors, which were subjected to periodic siRNA injection, starting from 2 weeks after transplantation of the cells. Each group has four mice. The error bars represent ± SEM.
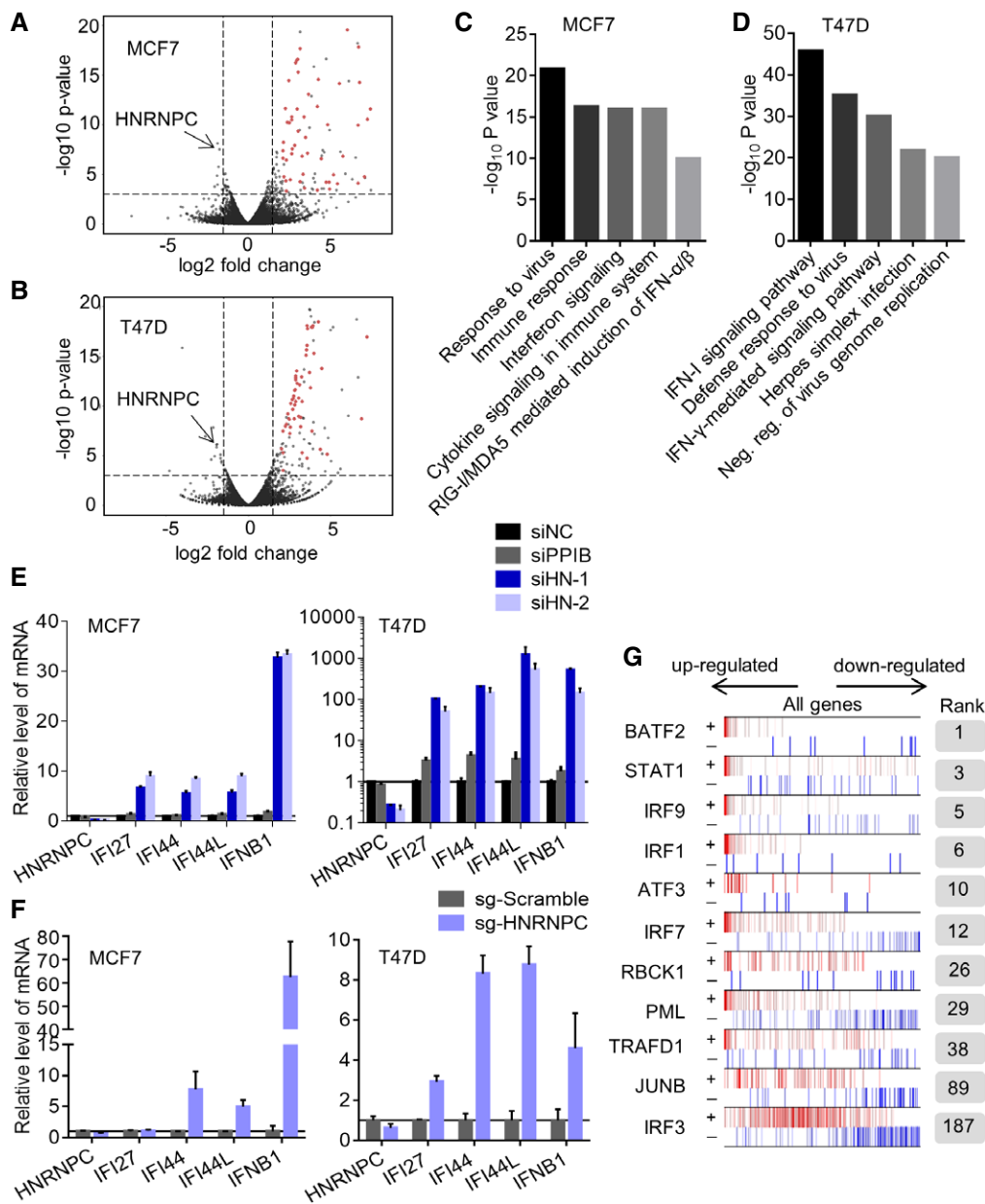
**Figure 2.  Repression of HNRNPC induced the interferon response and expression of ISGs in breast cancer cells.**

A, B  Volcano plots showing the differential expression of the genes after HNRNPC knock-down in the MCF7 (A) and T47D (B) cells. The ISGs with significant differential expression were marked as red dots. The cutoffs (dashed line) were set at the log2 fold change > 1.5 or < −1.5 and the $P < 0.001$.

C, D  Enrichment of the GO and KEGG functional annotations in the up-regulated gene sets upon HNRNPC knock-down in MCF7 (C) and T47D (D) cells. The *P*-values (−log10) of such enrichments were provided on the *y*-axis.

E, F  qPCR measurements of the expressions of ISGs upon knock-down of HNRNPC in MCF7 and T47D cells using siRNA (E) or CRISPR-Cas9 (F). Each sample has three replicates. Data represent mean ± SD.

G    11 TFs involved in the interferon response and signaling, which were identified by MARINa as master TFs upon HNRNPC knock-down. In each row, all genes were sorted (from left to right) by their differential expressions in siHNRNPC vs. control cells. The predicted target genes that are positive or negative regulated by the TF are marked as red or blue bars. All the TFs were sorted by the *P*-values (FDR-corrected) from the MARINa analysis. Ranks of these 11 TFs among all the master TFs identified by MARINa were provided to the right.

## IFNβ and the IFN signaling pathway mediated the arrestment of proliferation in response to HNRNPC knock-down

Considering the high level of IFNβ in the media after HNRNPC knock-down in MCF7 and T47D (Fig 3A), we transferred the media, 48

hours after the siRNA transfection of HNRNPC, to the wild-type cells without HNRNPC repression. These cells also gained elevated expression levels of the ISGs (Fig 3B), whereas neutralization of IFNβ by adding its antibody into the media resulted in significantly reduced responses of the ISGs in these cells (Fig 3C). The cell proliferation

**Figure 3. HNRNPC repression up-regulated the ISGs and suppressed MCF7 and T47D proliferation by activating the IFNβ production.**

A   Concentrations of IFNβ, measured by ELISA, in the culturing media of MCF7 and T47D cells 48 hours after siRNA transfections. siNC: non-targeting siRNA as a negative control, siHN-1: siRNA sequence 1 for HNRNPC, siHN-2: siRNA sequence 2 for HNRNPC, siLMNA: siRNA for LMNA as another negative control. Each sample has three replicates. Data represent mean ± SD.
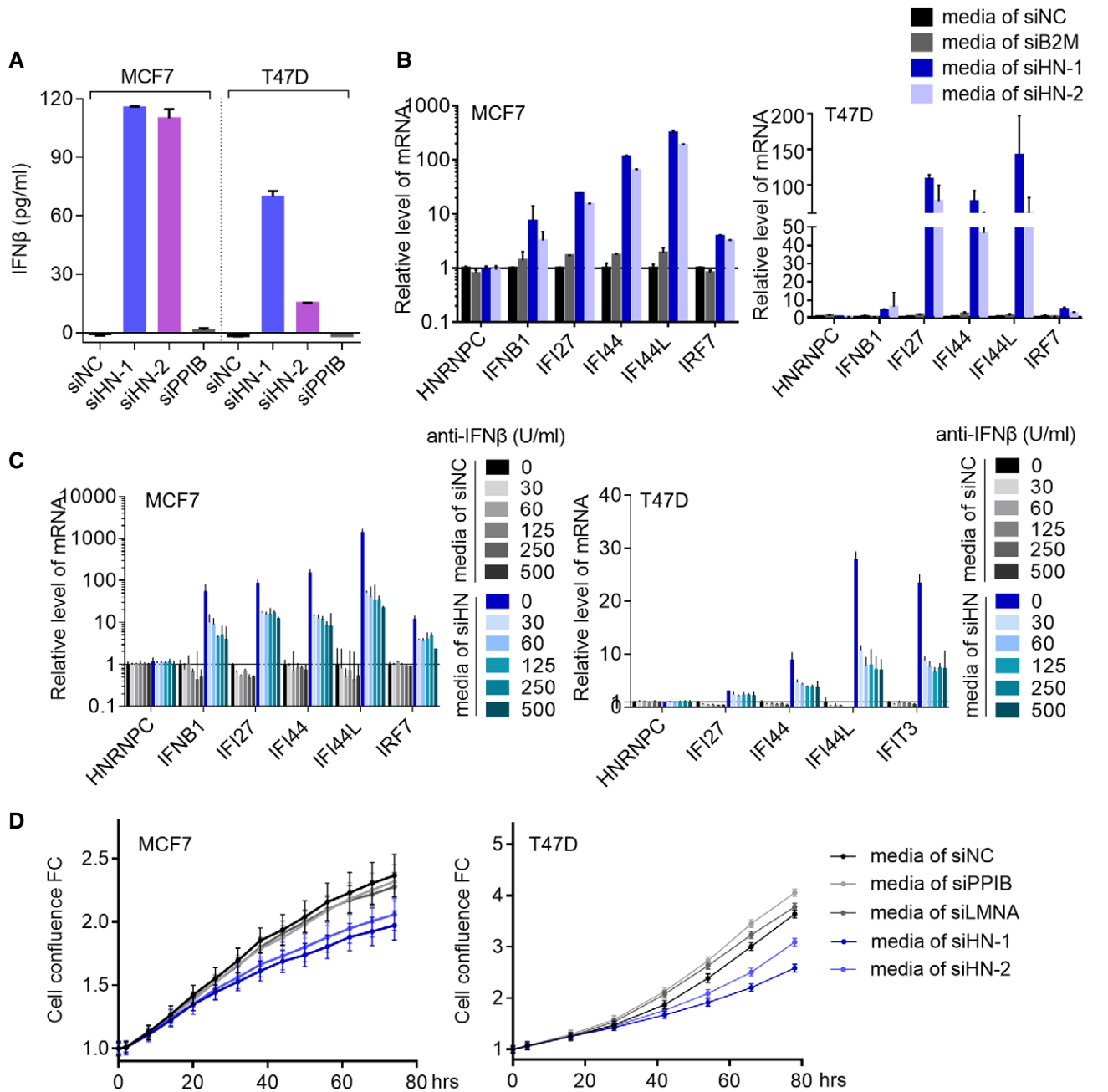
B   The normal MCF7 (left) and T47D (right) cells were cultured in the media collected from the corresponding cells 48 h after siRNA-mediated gene knock-down. Expressions of the ISGs in these normal cells were measured with qPCR. Each sample has three replicates. Data represent mean ± SD.

C   Different doses of the IFNβ antibody were added to the media of the siRNA-transfected MCF7 (left) or T47D (right) cells right before the media were transferred to the wild-type cells. The wild-type MCF7 or T47D cells were then cultured in these media for 48 hours, and the expressions of ISGs were measured by qPCR. Each sample has three replicates. Data represent mean ± SD.

D   Growth curves of the MCF7 (left) and T47D (right) cells cultured in the media collected from the siRNA-transfected cells. Each sample has three replicates. Data represent mean ± SD.

was also repressed in such media ($P < 0.01$, Fig 3D), which is similar to the effect of HNRNPC knock-down itself, even though the HNRNPC expression level remained unchanged (Fig 3B). Therefore, it is highly suspected that the cell proliferation-repressive effect of HNRNPC knock-down was indeed mediated by the secreted IFNβ and the subsequent activation of the type I interferon signaling pathway.

The well-studied type I interferon signaling pathway starts with binding of the extracellular IFNβ with the cell surface receptors IFNAR1/2, in which IFNAR2 is essential (Schreiber & Piehler, 2015; Lopez de Padilla & Niewold, 2016). In response to this binding signal, the JAK-STAT pathway is activated, leading to transcriptional up-regulation of the ISGs (Ivashkiv & Donlin, 2014; Schneider *et al*, 2014). Therefore, to show that the up-regulated ISGs upon HNRNPC knock-down depend on the interferon signaling cascade, we used an IFNβ antibody, an IFNAR2 blocking antibody, and the JAK-STAT inhibitor ruxolitinib to block the interferon signaling pathway at different levels. Indeed, disruptions of the interferon signaling pathway in the HNRNPC-repressed cells, by neutralization of the extracellular IFNβ, blockage of the membrane receptor IFNAR2, or inhibition of the JAK-STAT cascade, all attenuated up-regulations of the ISGs, including IFNB1, IFI27, IFI44, and IFI44L, in a dose-dependent manner (Fig 4A–C). In addition, more importantly, neutralization of IFNβ and inhibition of JAK-STAT both rescued the cell growth repression resulted from HNRNPC knock-down, in an antibody or inhibitor dose-dependent manner (Fig 4D–F). In fact, the high dosages almost completely offset the growth arrest effect of HNRNPC repression.

In summary, the results above have demonstrated that the anti-proliferation effects of HNRNPC repression in MCF7 and T47D cells can indeed be attributed to the production of IFNβ and the resulted activation of the type I interferon signaling pathway. Next, we sought to elucidate how repression of the RBP HNRNPC could lead to activation of such potent interferon responses.

### The dsRNA sensor RIG-I mediated the interferon response and tumorigenesis arrestment upon repression of HNRNPC

Under various stress conditions, abnormal accumulations of endogenous double- or single-stranded DNA or RNA may be sensed by cytoplasmic PRRS and trigger the interferon response (West *et al*, 2015; Roers *et al*, 2016), with effects on cell proliferation and the innate and adaptive immune systems (Chiappinelli *et al*, 2015; Roulois *et al*, 2015; Goel *et al*, 2017). Given that HNRNPC has been well known for its involvement in multiple RNA-related processes such as pre-mRNA splicing (Anantha *et al*, 2013), mRNA stabilization (Shetty, 2005), and RNA exportation (McCloskey *et al*, 2012), we looked into the RNA sensors for their potential involvements in mediating the interferon response upon repression of the normal HNRNPC function in MCF7 and T47D. RIG-I (gene name DDX58), melanoma differentiation-associated protein 5 (MDA5, gene name IFIH1), and Toll-like receptor 3 (TLR3) are three major dsRNA sensors in non-immune cells (Kawai & Akira, 2008). TLR3 is located on the cell and endosome membrane, and its mRNA expression level was barely detectable in MCF7 and T47D cells with either qPCR or RNA-seq. To test the involvements of the other two RNA sensors in the interferon responses upon HNRNPC repression, we prepared the MCF7 and T47D cells with stable knock-down of DDX58 or IFIH1 (Appendix Fig S7A). The up-regulations of IFNB1 and ISGs by HNRNPC knock-down were almost completely abrogated in the cells with repressed DDX58, but not in the cells with IFIH1 knock-down (Fig 5A). Consistently, IFNβ was not detected in the media of DDX58 knock-down cells after silencing HNRNPC, while the IFIH1 knock-down cells performed similar to the control cells in producing IFNβ upon HNRNPC repression (Fig 5B). Next, since MAVS is the central

mediator of the RIG-I-dependent signaling cascade leading to transcriptional activation of the IFNB1 gene (Kawai & Akira, 2008; Reikine *et al*, 2014), we further tested the involvement of MAVS in mediating the interferon response upon HNRNPC repression. Knock-down of MAVS indeed resulted in complete blockage of IFNB1 and ISG up-regulations upon HNRNPC repression (Appendix Fig S8), which is as potent as DDX58 silencing.

Furthermore, knock-down of DDX58, but not IFIH1, completely blocked the cell growth-inhibitory effect of HNRNPC silencing (Fig 5C). *In vivo* xenograft tumor models also confirmed that the MCF7 cells with DDX58 knock-down (Appendix Fig S7B) gained resistance to the tumor-inhibitory effect of HNRNPC repression (Fig 5D, compared to Fig 1G). Finally, in contrast to the result shown in Fig 1H, the xenograft tumors derived from the MCF7 cell with DDX58 knock-down were not any more responsive to periodic injection of the siRNA of HNRNPC (Fig 5E and Appendix Fig S7C).

In addition, there are also other ds/ssRNA sensors, such as OAS1-3 and IFIT1-5. Knocking-down any of these sensors could not block the up-regulation of ISGs or inhibition of proliferation upon HNRNPC repression (Appendix Fig S9A–E). Taken together, our results have shown that upon HNRNPC repression, the RIG-I-MAVS signaling pathway is responsible for triggering the cascade of IFNβ production and activation of the type I interferon signaling pathway, which leads to the up-regulated ISGs and eventually the tumor cell growth inhibition.

Finally, it is worth noting that the proposed machinery, RIG-I-mediated interferon response, is different than the non-specific siRNA-induced interferon response, which depends on activation of PKR (46) or TLR3 (47). The interferon response and arrestment of cell proliferation induced by HNRNPC repression were not sacrificed in the cells with stable knock-down of PKR (Appendix Fig S10A and B), indicating that the interferon response upon HNRNPC repression is not simply a non-specific immune response. Interestingly, as an ISG, PKR was up-regulated by HNRNPC silencing, at both the mRNA and protein levels (Appendix Fig S10C and D). Importantly, either neutralization of the IFNβ or stable knock-down of DDX58, which senses the dsRNA species and mediates the interferon response, completely abrogated the up-regulation of PKR induced by HNRNPC repression (Appendix Fig S10C and D). Therefore, the up-regulation of PKR expression is a consequence of the interferon response upon HNRNPC silencing.

### Repression of HNRNPC resulted in increase in the endogenous dsRNA

Given that RIG-I is one of the major dsRNA sensors and that HNRNPC is deeply involved in multiple RNA processing events, we were curious whether knock-down of HNRNPC could lead to an abnormal dsRNA accumulation, which should subsequently trigger the interferon signaling via RIG-I. Indeed, immunofluorescence (IF) staining for dsRNA using anti-dsRNA J2 antibody revealed a significant elevation of endogenous dsRNA in MCF7 and T47D upon HNRNPC KD (Fig 6A and Appendix Fig S11). Interestingly, MCF10A, BT549, or MDA-MB-231 cells did not show dsRNA increase upon HNRNPC silencing (Appendix Fig S12A–C), which is consistent with the resistances of these cells to HNRNPC repression, in their growth rates and levels of the interferon response (Appendix Figs S5 and S6).
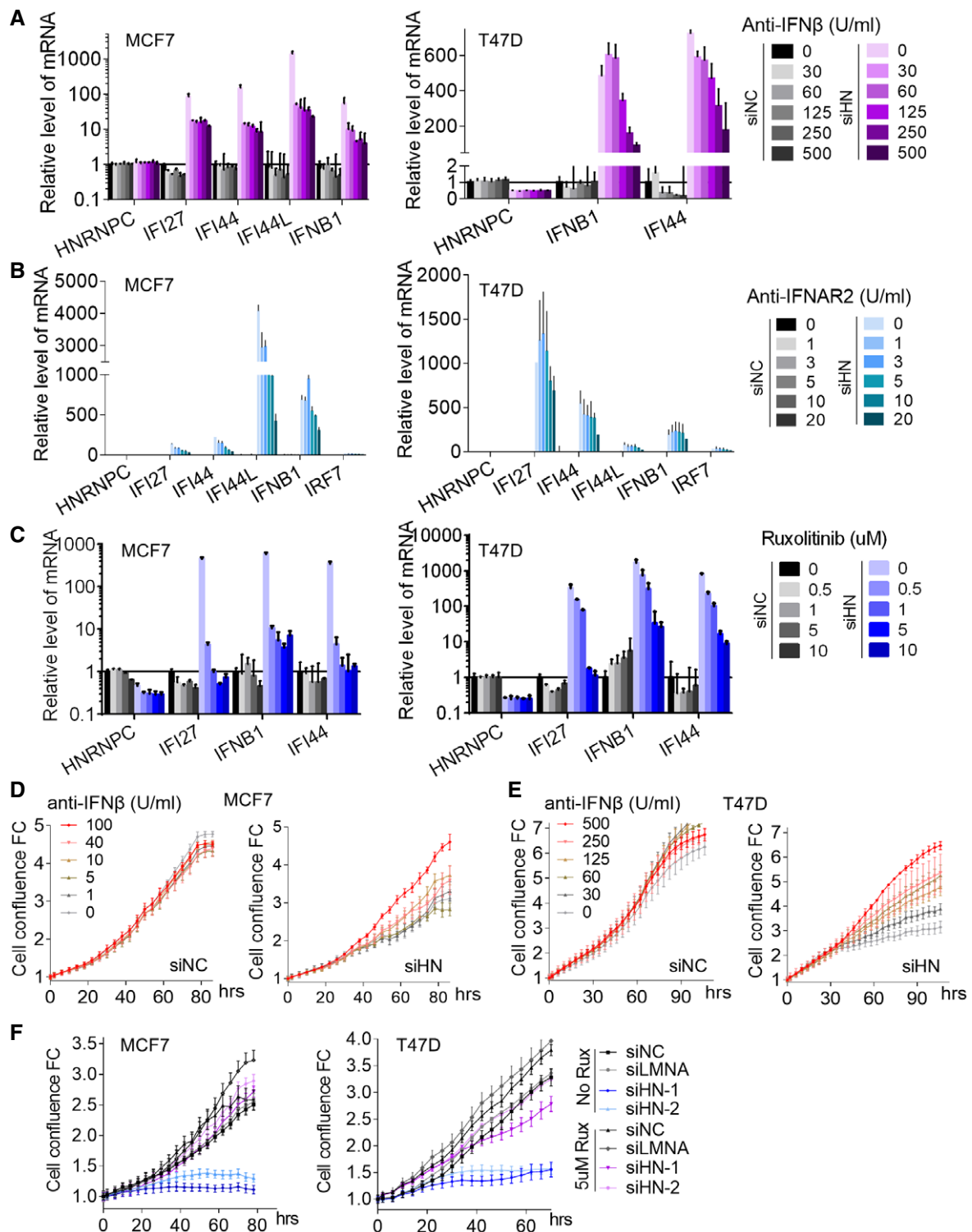
**Figure 4.  Up-regulated ISG expression and suppressed MCF7 and T47D proliferation upon HNRNPC repression mediated via the interferon beta signaling pathway.**

A–C    In the siRNA-transfected MCF7 (left) or T47D cells (right), the interferon signaling pathway was blocked at different stages by means of IFNβ neutralization (A), IFNAR2 neutralization (B), or JAK-STAT inhibition (C). The expressions of the ISGs were measured by qPCR. Each sample has three replicates. Data represent mean ± SD.

D, E    Growth curves of the MCF7 (D) or T47D cells (E) upon HNRNPC knock-down but with the interferon response blocked with the IFNβ antibody. Each sample has three replicates. Data represent mean ± SD.

F    Growth curves of the MCF7 (left) or T47D (right) cells upon HNRNPC knock-down and JAK-STAT inhibition with ruxolitinib (5 μM). siNC: non-targeting siRNA as a negative control, siLMNA: siRNA for LMNA as another negative control, siHN-1: siRNA sequence 1 for HNRNPC, siHN-2: siRNA sequence 2 for HNRNPC. Each sample has three replicates. Data represent mean ± SD.
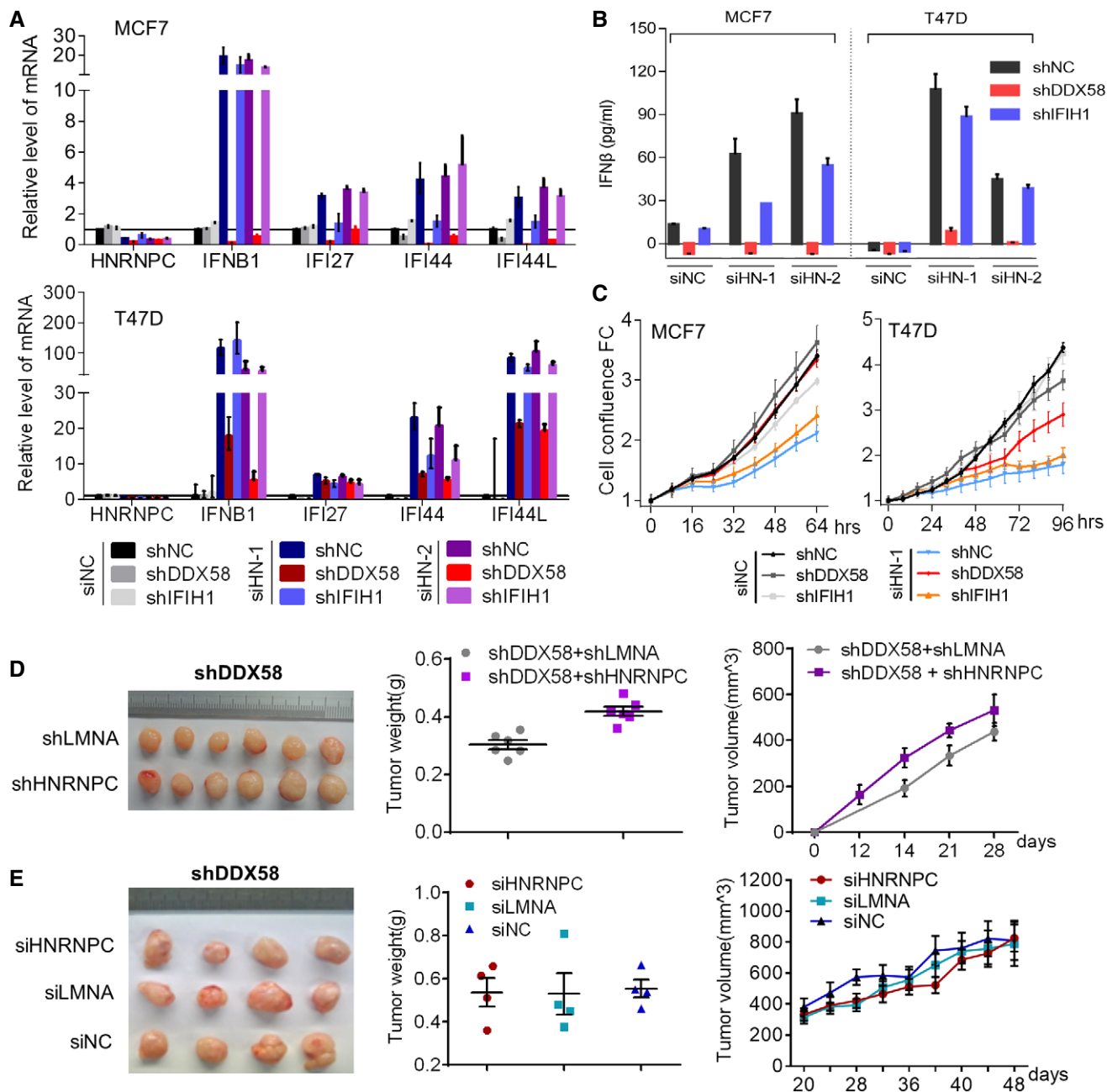
**Figure 5.   The interferon response and tumor-inhibitory effect of HNRNPC repression were mediated via the dsRNA sensor RIG-I (DDX58).**

A, B    Expression levels of ISGs (A) and IFNβ concentration in the media (B) upon HNRNPC silencing in the cells with lentiviral shRNA-mediated stable knock-down of DDX58 or IFIH1. Each sample has three replicates. Data represent mean ± SD.

C    Growth curves of the DDX58- and IFIH1-deficient MCF7 (left) and T47D (right) cells upon HNRNPC knock-down. Each sample has three replicates. Data represent mean ± SD.

D    Xenograft tumor models with DDX58-deficient MCF7 cells. Images, weights, and growth records of the xenograft tumor models in female NSG mice established from the DDX58-deficient MCF7 cells upon lentivirus-mediated stable knock-down of LMNA or HNRNPC. Each group has six mice. The error bars represent ± SEM.

E    Xenograft tumor models with DDX58-deficient MCF7 cells. Images, weights, and growth records of the xenograft tumors derived from DDX58-deficient MCF7 cells, which were subjected to periodic siRNA injection, starting from 2 weeks after transplantation of the cells. Each group has four mice. The error bars represent ± SEM.

We then sought to systematically identify and profile these dsRNA species. As shown above, RIG-I, which recognizes relatively short (< 300 bp) cytoplasmic dsRNA (Schlee & Hartmann, 2016), serves as the main mediator of the interferon response upon HNRNPC KD, while MDA5, which senses longer dsRNA (DeWitte-Orr & Mossman,

2010; Wu *et al*, 2013; Reikine *et al*, 2014), was not involved (Fig 5). Therefore, we are interested in the pool of short (< 500 bp) dsRNA species and developed a strategy to pull down the short dsRNA with the anti-dsRNA J2 antibody from the total RNA. The dsRNA-enriched libraries from different cells were then sequenced, followed by a
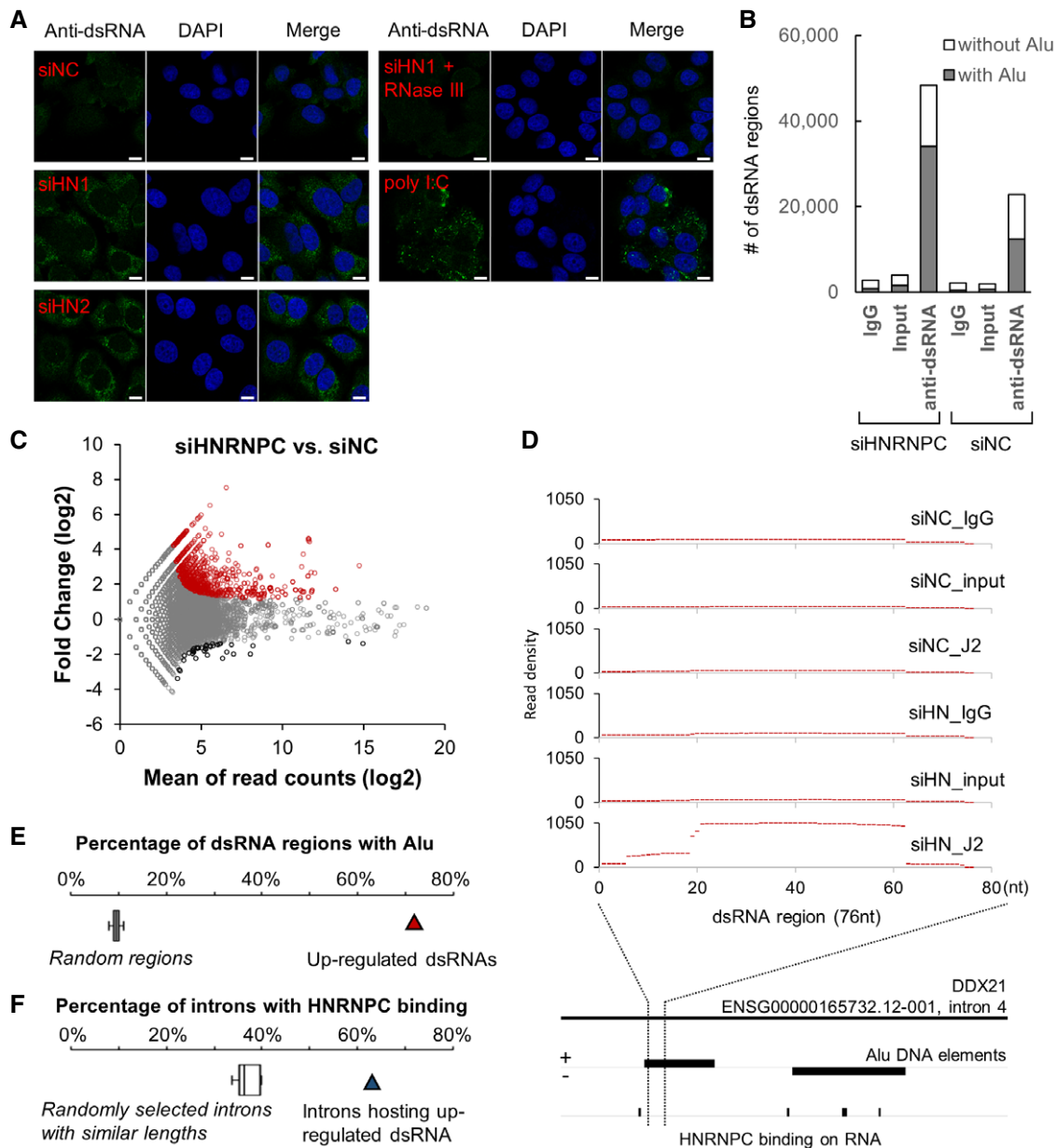
**Figure 6.  Repression of HNRNPC resulted in elevation of endogenous dsRNA.**

A  Immunofluorescence analysis of the dsRNA in MCF7 cells after knock-down of HNRNPC, with 4′,6-diamidino-2-phenylindole (DAPI) staining (blue) and anti-dsRNA antibody J2 (green). Cells transfected with poly I:C was included as a positive control of dsRNA, and the cells treated with RNase III was used as a negative control. siNC: non-targeting siRNA as a negative control, siHN-1: siRNA sequence 1 for HNRNPC, siHN-2: siRNA sequence 2 for HNRNPC. The size of scale bar is 10 μm.

B  Counts of dsRNA regions in the siNC control cells or in the cells with siHNRNPC, identified in the dsRNA-enriched libraries with anti-dsRNA J2 pull-down or in the control libraries including the IgG control and the input control for dsRNA pull-down. Each bar represents the overlapping dsRNA species from two replicate experiments. Among each set of the dsRNA regions, the dsRNAs from Alus were marked in gray.

C  MA plot showing all the dsRNA regions identified in the dsRNA-enriched libraries. For each dsRNA region, mean of the read counts (log2) for two replicates of siHNRNPC and siNC cells was shown on the *x*-axis, and the average fold change (log2) in siHNRNPC vs. siNC on the *y*-axis. The up-regulated dsRNA regions were marked in red and down-regulated regions in black.

D  An example of the up-regulated dsRNA regions upon HNRNPC knock-down. On top of the figure are plots of the read densities along the dsRNA region, in the dsRNA-enriched libraries (J2) and the two control libraries (IgG and input), from the siNC and siHNRNPC cells. This dsRNA region was originated from intron 4 of DDX21 transcript ENSG00000165732.12-001, which is shown at the bottom of the figure. The Alu DNA elements and the HNRNPC binding regions in this intron were also marked.

E  From the results of RepeatMasker, percentage of the up-regulated dsRNA regions (928 regions highlighted in panel C) was counted that contain or largely overlap with the Alu elements. For comparison, repeated for 10 times, the same number of intra-genic regions was randomly selected and the percentage of Alu was counted with RepeatMasker. The results, i.e., percentages of Alu in these 10 random sets, were summarized as box plot.

F  Percentage of the introns harboring the up-regulated dsRNA regions (698 introns in total, accounting for 864 of the 928 regions shown in panel C) that contain the previously identified HNRNPC binding regions. For comparison, 10 sets of randomly selected introns, which have the same length distributions as the 698 introns, were also queried. The results, i.e., percentages of the introns containing the HNRNPC binding regions in these 10 random sets, were summarized as box plot.

series of bioinformatics analyses for filtering the reads and identifying the dsRNA species in the transcriptome.

Such dsRNA profiling procedure was designed to capture the "free" dsRNA species but not the dsRNA structures embedded in longer RNA molecules such as mRNAs. It has been well acknowledged that long mRNA and non-coding RNA species harbor many dsRNA regions as basic elements of their secondary structures, e.g., "stems" in stem-loops (Svoboda & Di Cara, 2006; DeWitte-Orr & Mossman, 2010). These intra-molecular dsRNA structures lack phosphorylated 5′ ends, which makes them impotent for triggering the RIG-I-mediated interferon response (Sun et al, 2012; Reikine et al, 2014). However, these embedded dsRNA structures might interfere with the J2 antibody and therefore could be pulled down by J2 (Schonborn et al, 1991; Kaneko et al, 2011). In fact, we did try IP with J2 without size selection of the RNA. As suspected, the RNA pulled down was dominated by long RNA species, and the overall length distribution was similar to the total RNA input (data not shown). Furthermore, quantifications of the RNA pulled down by J2 showed no significant difference in HNRNPC KD and the negative control cells. As discussed above, this is not surprising. The RNA pulled down was dominated by long RNA molecules with base-paired structures, which resulted in an unacceptably high background noise for quantitative comparison of the immunostimulatory free dsRNA species. Therefore, we believe that it is necessary to separate and enrich the small RNA species (< 500 bp) first, followed by IP with J2.

Interestingly, our dsRNA-seq strategy recovered short, free dsRNA species (< 100 nt) (Fig EV2A), even though our size selection was performed around 500 nt. Compared to the total RNA input and the IgG control, the libraries pulled down by anti-dsRNA J2 did recover much more dsRNA regions (Fig 6B), which are twice as abundant in the HNRNPC knock-down cells as in the control cells (Fig 6B). These dsRNA species were mostly originated from introns of long mRNA or non-coding RNA molecules (Fig EV2B). Quantifications of the dsRNA abundances showed that knock-down of HNRNPC indeed resulted in up-regulation of many dsRNA regions (928 regions, marked red in Fig 6C), most of which (864 out of 928) are located in introns of the mRNAs and long non-coding RNAs (Fig EV2C). An example of the up-regulated dsRNA regions, originated from an intron of a pre-mRNA, is shown in Fig 6D. It is worth noting that such dsRNA up-regulation was not associated with the general transcriptional up-regulation of the host genes. In fact, most of the host genes of these dsRNA regions did not have any type of differential expression upon HNRNPC knock-down (Fig EV2D).

RIG-I, but not MDA5, primarily recognizes RNA targets with triphosphorylated 5′ end (5′ppp) (Wang et al 2010; Baum et al 2010; Peisley et al 2012), and recent studies reported that RNA with diphosphorylated 5′ end (5′pp) are substrates of RIG-I as well (Goubau et al, 2014). Therefore, we have performed enrichment of 5′ppp RNA followed by RNA sequencing to query the dsRNA species identified with J2 dsRNA-seq and to quantify the percentage of the dsRNAs that have 5′ppp. Strikingly, most of the up-regulated dsRNA species upon HNRNPC KD have 5′ppp ends (Fig EV3A), which strongly supports our hypothesis of RIG-I-mediated interferon response. In addition, our previous experiments of DDX58 KD showed that repression of DDX58 significantly reversed the interferon response activated by HNRNPC KD. Here, further rescue experiments, with wild-type RIG-I or RIG-I with its 5′ppp RNA recognition domain mutated or truncated (Fig EV3B), confirmed

that the 5′ppp RNA recognition function of RIG-I is responsible for triggering interferon response upon HNRNPC KD (Fig EV3C). Importantly, stable knock-down of DDX58 did not affect the accumulation of dsRNA upon HNRNPC silencing (Appendix Fig S13), confirming that the elevated dsRNA was not a by-product of interferon response.

In summary, our results have shown that the dsRNA sensor RIG-I mediated the interferon response and tumor growth arrest upon HNRNPC repression in breast cancer cells MCF7 and T47D, which is well in line with the significant accumulation of immunostimulatory endogenous dsRNA species upon knock-down of HNRNPC.

## Characterization of the dsRNA species induced by HNRNPC repression

Surprisingly, the up-regulated dsRNA species upon knock-down of HNRNPC are very highly enriched by the Alu elements. 71% of these dsRNA regions contain or largely overlap with Alu sequences, compared to just about 10% for the randomly selected intra-genic regions with similar length distributions (Fig 6D and E for an example). In fact, it has been shown that Alu RNAs composed the major form of dsRNA under certain pathological contexts (Kaneko et al, 2011) and that the adenosine deaminase ADAR1 destabilizes dsRNA structures from Alu sequences in pol II-transcribed mRNA via RNA editing (Chung et al, 2018). Here, we found that silencing ADAR1 only did not alter the ISGs or cell proliferation rate (Fig EV4A and B), whereas silencing ADAR1 together with HNRNPC resulted in elevated ISG signatures and stronger inhibition of cell proliferation (Fig EV4C and D). These observations are consistent with our finding that repression of HNRNPC primarily functions on Alu-enriched dsRNA species.

Heterogeneous nuclear ribonucleoprotein C has been well characterized for its function in binding to the intron regions of pre-mRNA and regulating silencing or inclusion of the introns (Konig et al, 2010). Further studies revealed that HNRNPC is essential for repression of aberrant exonization of the Alu elements in the introns, and loss of HNRNPC resulted in abnormal inclusion of Alu in the transcripts (Zarnack et al, 2013). Therefore, we suspect that the newly discovered dsRNA-controlling function of HNRNPC is a consequence of the well-appreciated function of HNRNPC in regulating RNA splicing. Indeed, the harboring introns of these up-regulated dsRNA regions, compared to the randomly selected intron sets with similar length distributions, are much more enriched by the previously identified RNA binding sequences of HNRNPC (Konig et al, 2010; Zarnack et al, 2013) (Fig 6F), suggesting co-occurrence of HNRNPC binding and dsRNA origination in the introns.

We propose that HNRNPC ensures the proper RNA metabolism and splicing, whereas reduction in HNRNPC impairs such normal processes and results in RNA transcripts with aberrant exonization of Alu introns. These transcripts are subjected to cytoplasmic RNA quality control mechanisms, e.g., nonsense-mediated decay (NMD) of mRNAs with premature stop codons or truncated open reading frames (Zarnack et al, 2013; Attig et al, 2016), and thereby give rise to dsRNA fragments as a by-product. Regulator of nonsense transcripts 1 (UPF1) is required for such RNA recycle machinery (Popp & Maquat, 2014). Indeed, knocking-down UPF1 in addition to HNRNPC in the MCF7 cells almost completely abrogated the dsRNA

accumulation due to HNRNPC repression (Fig EV5A). As a result, the dramatic activation of IFNβ mRNA expression upon silencing of HNRNPC was significantly reduced, almost to the control level (Fig EV5B). Considering that UPF1 also mediates the STAU1-mediated mRNA decay (SMD; Kim *et al*, 2005), which degrades mRNA with a STAU1 binding site in the 3′ UTR (Kim *et al*, 2007), we tested whether SMD also contributed to the dsRNA accumulation. In contrast, knocking-down STAU1 did not reduce the endogenous dsRNA (Fig EV5A) or the IFNβ mRNA expression (Fig EV5B) upon HNRNPC repression, suggesting that SMD was not involved in the process of dsRNA accumulation here.

Furthermore, SMG6 is the endonuclease during NMD, which cleaves the NMD targets and initiates exonucleolytic decay of the RNA degradation intermediates from both the 5′ and 3′ ends (Schmidt *et al*, 2015; Hug *et al*, 2016; Kurosaki & Maquat, 2016). We then performed SMG6 knock-down (Appendix Fig S14A) and showed that similar to UPF1, repression of SMG6 significantly reduced the ISG up-regulation in response to HNRNPC knock-down (Appendix Fig S14B). Consistently, the cell proliferation rate was also rescued by knocking-down SMG6 or UPF1 (Appendix Fig S14C). Collectively, the results above suggest that the NMD machinery is deeply involved in mediating the accumulation of dsRNA and the down-stream interferon response upon HNRNPC repression. Therefore, we propose that dysregulated alternative splicing upon HNRNPC KD resulted in NMD of the Alu-enriched transcripts, which eventually generated Alu dsRNAs and triggered RIG-I-mediated interferon response.

# Discussion

Elevated expression of HNRNPC has been reported in multiple types of cancer cells (Pino *et al*, 2003; Sun *et al*, 2007; Park *et al*, 2012; Mulnix *et al*, 2014), but the physiological function of HNRNPC in tumorigenesis has not been fully understood. In the present study, we showed the indispensable role of HNRNPC in the breast cancer cells MCF7 and T47D (Fig 1). Repression of HNRNPC, by means of RNAi or CRISPR-mediated knock-down, greatly suppressed cell proliferation and *in vivo* tumor growth. Even direct injection of the packaged siRNA of HNRNPC into the xenograft tumors, which only resulted in partial knocking-down, exhibited significant suppression of tumor growth. Such vulnerability of MCF7 and T47D suggests a potential oncogene addiction of breast cancer and hints at a new potential therapeutic strategy of HNRNPC repression. However, our results have also raised an intriguing question: how would the dsRNA accumulation and the subsequent activation of the interferon response in the tumor cells interact with the tumor microenvironment, especially with the tumor-infiltrating lymphocytes (Chiappinelli *et al*, 2015; Goel *et al*, 2017)? In the future study, it would be very interesting to test whether such tumor-inhibitory function of HNRNPC repression would be further enhanced in the real tumor microenvironment.

The RBP HNRNPC has attracted much attention in the recent years, for its multiplex functions in regulating pre-mRNA splicing (Konig *et al*, 2010; Zarnack *et al*, 2013), mRNA stabilization (Shetty, 2005), length-dependent exportation (McCloskey *et al*, 2012), stability and translation (Holcik *et al*, 2003; Kim *et al*, 2003; Schepens *et al*, 2007), etc. Although HNRNPC has been shown to regulate multiple cancer-related genes, mostly through RNA-related processes, understanding about the accountable machinery for the function of HNRNPC in tumors is still limited. By combining a series of high-throughput profiling, data-mining, and systematic computational inference of the driving TF pathway, our study discovered a surprising yet strong signature of activated interferon response and interferon signaling upon repression of HNRNPC (Fig 2). Furthermore, a series of experiments blocking the first wave of interferon responses and the second wave of interferon signaling at various stages all confirmed that such process is indeed the primary machinery mediating the tumorigenesis-inhibitory effect of HNRNPC repression (Figs 3 and 4). Finally, we showed that upon perturbation of HNRNPC, the pre-mRNA introns gave rise to dsRNA, which triggered the interferon response and tumor growth arrestment. However, a question remained unanswered, i.e., why certain cancer cells might have higher needs for HNRNPC? In fact, the requirement of HNRNPC seems context-dependent, and we do not have a definitive explanation yet. In a mouse model, HNRNPC is dispensable for viability of mouse embryonic stem cells established from homozygous mutant blastocysts (Williamson *et al*, 2000). For the different types of cells that we tested, silencing HNRNPC is inhibitory to MCF7 and T47D but not to the other tumor cell lines (MDA-MB-231 and BT549) or non-tumor cell MCF10A. Interestingly, knocking-down HNRNPC failed to induce interferon response and dsRNA accumulation in these non-responsive cells as well. This suggests that there could be a complementary machinery that helps retaining the control of interferon response and dsRNA accumulation by compensating for loss of HNRNPC in these cells. HNRNPC repression is well known to induce alternative splicing. Therefore, such compensating machinery may monitor the RNA post-transcriptional processing and block dsRNA generation even if some pre-mRNAs were subjected to alternative splicing. This hypothesis certainly worths further investigation. Nevertheless, the critical function of HNRNPC in breast cancer cells MCF7 and T47D is well supported by our results.

The physiological function of dsRNA-induced IFN in cancer could be complicated. A previous study suggested that activation of stromal NOTCH-MYC by breast cancer cells results in production of unshielded RN7SL1 in exosomes (Nabet *et al*, 2017). exoRNA RN7SL1 was then transferred to breast cancer cells, activated RIG-I signaling including STAT1 activation and ISG induction, which was proposed to promote aggressive development of cancer. In another work, the same group has demonstrated that RIG-I activation by exoRNA can amplify NOTCH3 signaling, which is responsible for the expansion of tumor-initiating cells and therapy resistance in ISG-R breast cancer cells, which are mostly basal/triple-negative breast cancer (TNBC) cells (Boelens *et al*, 2014). However, in our work done in different types of breast cancer cells, expression profiles of the down-stream genes indicated that NOTCH3 signaling was not amplified when interferon signaling was activated. On the other hand, several other studies have reported that up-regulated dsRNA from endogenous retrovirus (ERV) in tumor cells, triggered by DNA methyltransferase inhibitors or CDK4/6 inhibitors, induced IFN responses and thus inhibited tumor development (Chiappinelli *et al*, 2015; Roulois *et al*, 2015; Goel *et al*, 2017). Our proposed model is similar to these studies, even though the dsRNA species in our study were originated from a different resource than ERV.

Endogenous dsRNA species are some of the primary activators of the interferon response (Leonova *et al*, 2013; Mannion *et al*, 2014; White *et al*, 2014; Chiappinelli *et al*, 2015; Liddicoat, 2015; Roulois *et al*, 2015; Goel *et al*, 2017). Recent studies showed transcriptional activations of the ERVs triggered by several anti-tumor drugs, which in turn resulted in ERV-originated dsRNA accumulation, potent interferon responses, and significant tumor inhibition (Chiappinelli *et al*, 2015; Roulois *et al*, 2015; Goel *et al*, 2017). In contrast, our study showed that upon perturbation of the RBP HNRNPC, the non-ERV pre-mRNA introns gave rise to dsRNA, which triggered the interferon response and tumor growth arrestment as well. We believe that such a completely different machinery of dsRNA origination, but with a similar down-stream tumor-inhibitory effect, worths further investigations for more mechanistic details. Interestingly, these up-regulated dsRNAs are highly enriched by the Alu elements, and the dsRNA-hosting introns are enriched by the known HNRNPC binding sequences. Considering the previous finding that loss of HNRNPC resulted in abnormal exonization of Alu introns (Konig *et al*, 2010; Zarnack *et al*, 2013), which could trigger the NMD pathway (Attig *et al*, 2016), we proposed that the immunostimulatory dsRNA species were originated from the NMD pathway. Indeed, our data showed that the two critical factors for initiation of the NMD pathway, UPF1 and SMG6, are required for the interferon response upon HNRNPC repression. SMG6 has endonuclease activity, which results in direct cleavage of the NMD targets and initiation of the exonucleolytic RNA decay from both the 5′ and 3′ ends (Eberle *et al*, 2009; Schmidt *et al*, 2015; Hug *et al*, 2016; Kurosaki & Maquat, 2016). Therefore, we propose that the Alu dsRNA sequences are end products of a series of RNA decay processes, rather than just direct products of SMG6.

Our profiling of the 5′ triphosphorylated RNA showed that the accumulated dsRNA species upon HNRNPC repression have a strong preference to 5′ppp modifications, which is in line with the critical role of RIG-I in mediating the interferon response. However, it remains unclear how the dsRNA species gain such 5′ppp modifications. As discussed above, the dsRNAs are mostly from pre-mRNA introns and very likely products of RNA decay including the NMD. There is a disconnection between RNA decay and potential processing of the dsRNA species at 5′ ends. We suspect that these dsRNA products may be subjected to 5′ triphosphorylation via some phosphotransferases or even ribozymes (Moretti & Muller, 2014). This question is certainly interesting to pursue in future.

Finally, although the multiple pieces of data have consistently supported the model of RIG-I-mediated interferon response triggered by small dsRNA species as products of RNA decay upon HNRNPC repression, our data do not completely preclude potential alternative sources of immunostimulatory RNA species. To enrich for dsRNA and eliminate background noise of the dsRNA-seq assay, we performed total RNA extraction and size selection (< 500 nt). It is possible that some other dsRNA structures were also involved in stimulating the IFN response, for example the primary Alus transcribed by Pol III (Nabet *et al*, 2017). Even though the primary Alu transcripts are usually expressed at low levels (Hasler *et al*, 2007; Deininger, 2011), it is worth noting that our dsRNA enrichment and recovery procedure could miss some of these species. A more comprehensive profiling of all the RNA species resulted from the largely shifted transcriptome and dysregulated post-transcriptional RNA processing would be highly beneficial for fully understanding the impact of HNRNPC repression in different cancer cells.

In summary, the present study established the indispensable role of HNRNPC for tumorigenesis of the breast cancer cells MCF7 and T47D. Repression of HNRNPC resulted in potent arrestment of cell proliferation and tumor growth. Such tumor-inhibitory effect of HNRNPC knock-down was mediated through the cascade of interferon response, which was triggered by elevated endogenous dsRNA upon HNRNPC repression. These dsRNA species were originated from the Alu-enriched introns subjected to alternative splicing regulated by HNRNPC. Such machinery connects an individual RBP to the immune responses of tumor cells via dysregulated endogenous RNA processing in cancer. Our study sheds lights on how dysregulation of a RBPs may contribute to crafting the tumor microenvironment, and it would be particularly interesting to see whether other RBPs would also execute the same function via different or the same machineries.

## Materials and Methods

### Cell culture

Cells were purchased from the American Type Culture Collection (ATCC). MCF7 was cultured in Dulbecco's modified Eagle's medium (DMEM) (low glucose; Corning) supplemented with 10% FBS (HyClone). T47D and BT549 were grown in RPMI 1640 (Corning) with 10% FBS and 0.2 U/ml insulin. HEK293T cells were cultured in DMEM (high glucose) with 10% FBS. MDA-MB-231 was maintained in Leibovitz's L-15 medium (Gibco) with 10% FBS. MCF10A was cultured in DMEM/F12 medium supplemented with 5% horse serum, 10 mg/ml insulin, 0.5 mg/ml hydrocortisone, 20 ng/ml recombinant epidermal growth factor, 100 ng/ml cholera toxin, and 1% antibiotics (Lonza). Cells were maintained in a humidified incubator with 5% $CO_2$ at 37°C.

### Treatments of the chemicals and antibodies

Ruxolitinib (2 mM) (Invivogen), 0–20 U/ml of IFNAR2 antibody (PBL Interferon Source 21385-1), 0–500 U/ml of IFNβ antibody (PBL Interferon Source 31401-1) were added when changing the medium 6 h after siRNA transfection. For antibody blocking assay in media, cell media were collected 48 h after siRNA transfection and transferred to the normal cells, when different dosages of IFNβ antibody were added.

### siRNA transfection

Reverse transfections of the siRNAs (10 nM) were performed using Lipofectamine RNAiMAX Reagent (Invitrogen) following the manufacturer's instructions. siRNAs and RNAiMAX were separately diluted in opti-MEM and mixed together for 20 min at room temperature. For 96-well plates, 100 μl medium containing $10^5$ cells was added to the transfection mixture. Six hours after transfection, the supernatant was replaced with fresh cell medium. The siRNAs were purchased from GenePharma Co., Ltd. (Shanghai, China). The

sequences of the siRNAs used in the present study are listed in the following table. Scrambled siRNA as a non-targeting control (siNC) and the siRNAs targeting B2M, PPIB, or LMNA were used as negative controls.

| Gene name | Sense (5′–3′) | Antisense (5′–3′) |
|---|---|---|
| HNRNPC-1 | GCCUUCGUUCAGUAUGUUAAU | AUUAACAUACUGAACGAAGGC |
| HNRNPC-2 | GCGCUUGUCUAAGAUCAAAUU | AAUUUGAUCUUAGACAAGCGC |
| B2M | CUGGUCUUUCUAUCUCUUGUA | UACAAGAGAUAGAAAGACCAG |
| PPIB | CCUACGAAUUGGAGAUGAAGA | UCUUCAUCUCCAAUUCGUAGG |
| LMNA | GAAGCAACUUCAGGAUGAGAU | AUCUCAUCCUGAAGUUGCUUC |
| NC | UUCUCCGAACGUGUCACGU | ACGUGACACGUUCGGAGAA |
| STAU1 | GAGGAGAAGACACCCAUAAAG | CUUUAUGGGUGUCUUCUCCUC |
| STAU2 | GCCAGGGAACUCCUUAUGAAU | AUUCAUAAGGAGUUCCCUGGC |
| UPF1 | GAUGCAGUUCCGCUCCAUU | AAUGGAGCGGAACUGCAUC |
| OAS1 | CCUGUCAAAGAGAGAGAGCAU | AUGCUCUCUCUCUUUGACAGG |
| OAS2 | CCCACCAAACUAAAGGAUUUA | UAAAUCCUUUAGUUUGGUGGG |
| OAS3 | GGCAGUUCGAGGUCAAGUUUG | CAAACUUGACCUCGAACUGCC |
| IFIT1 | CUUCGGAGAAAGGCAUUAGAU | AUCUAAUGCCUUUCUCCGAAG |
| IFIT2 | GCAACCUACUGGCCUAUCUAA | UUAGAUAGGCCAGUAGGUUGC |
| IFIT3 | GCGAUGUACCAUCUGGAUAAU | AUUAUCCAGAUGGUACAUCGC |
| IFIT5 | GCAGAAGAAAUAAUCCAGCAA | UUGCUGGAUUAUUUCUUCUGC |
| SMG6 | CGCUCAGACAAACGAAGGAAU | AUUCCUUCGUUUGUCUGAGCG |
| ADAR1 | CGCAGAGUUCCUCACCUGUA | TACAGGTGAGGAACTCTGCG |

### shRNA lentivirus production and infection

The shRNA (MISSION® RNAi, SIGMA) plasmids were co-transfected with lentivirus packaging plasmid VSVG and Δ8.9 to HEK293T cells using Lipofectamine 2000. Six hours after transfection, the medium was replaced with DMEM (high glucose) with 10% FBS. The viral particles were harvested 72 h after transfection. Polybrene (8 μg/ml) was used to facilitate the lentivirus infections of MCF7 and T47D. 48 h after infection, puromycin (4 μg/ml) was added to the cell media for selection of the stably infected cells over multiple passages. The TRC IDs of the shRNAs are provided in the following table. Scrambled shRNA as a non-targeting control (siNC) and the siRNAs targeting PPIB or LMNA were used as negative controls.

| Gene name | TRC_ID | Gene name | TRC_ID |
|---|---|---|---|
| NC | SHC002 | IFIH1 | TRCN0000050849 |
| HNRNPC | TRCN0000006646 | PPIB | TRCN0000296764 |
| TLR3 | TRCN0000056851 | LMNA | TRCN0000061835 |
| DDX58 | TRCN0000153712 | MAVS | TRCN0000236031 |

### Tet-on CRISPR/Cas9-mediated knock-down

Lentiviral expression vectors for Tet-on CRISPR/Cas9 and sgRNA were purchased from Addgene (pCW-Cas9 50661; pLX-sgRNA 50662). The constructs were separately mixed with the packaging plasmid psPAX2 and VSVG and transfected to HEK293T cells using the Lipofectamine 2000 reagent (Invitrogen). The lentivirus in the medium was concentrated and transfected to MCF7 or T47D cells in the presence of 8 μg/ml polybrene. Puromycin and blasticidin were used to select for stable cell lines over 1 week. 10 μg/ml doxycycline was used to induce the expression of Cas9. Following are the sequences of the sgRNAs used in the present study: Scramble sgRNA (GCACTCACATCGCTACATCA), HNRNPC #1 sgRNA (GATCTGCAGCGGAGATGTAC), HNRNPC #2 sgRNA (TGAGTAGAGGGGACGGAGAA), and LMNA sgRNA (GGTAAGCCCAGTGAAACGTG) as a negative control.

### Cell proliferation assay

The normal cells or the cells after gene knock-down were cultured in 96-well plates, at the starting density of 10,000 cells per well. The IncuCyte® live-cell imaging and analysis system (ESSEN bioscience) was used to monitor the long-term cell growth and morphology change. Cell proliferation was quantified by measuring the occupied area (% confluence) of the cell images over time.

### Anchorage-independent colony formation assay

MCF7 and T47D cells stably expressing the shRNAs were collected, resuspended in culturing media containing 10% FBS and 0.3% agarose (Amresco), and then seeded on top of 0.6% agarose gel containing 10% FBS in six-well plates. The starting point of cell density was 1,000 cells per well. The cells were cultured in regular media for 3–4 weeks, and the colonies were stained with 0.005% crystal violet and photographed.

### Xenograft assays

Female immune-deficient NSG mice were supplemented with 17β-estradiol pellets (Innovative Research of America, 0.72 mg estradiol) one day before transplantation of the cells. After selection with antibiotics, 5 million cells suspended in 200 μl PBS with stable gene knock-down were subcutaneously injected to the mice. For siRNA injection, the shDDX58/shNC MCF7 cells were subcutaneously injected to the mice. The interventions with siRNAs were started on the 14th day after cell injection, when the transplanted tumors had grown to approximately 200–300 mm³. Specifically, 20 μg siRNA mixed with 10 μl *in vivo* RNA transfection reagent (Engreen Biosystem, Entranster-*in vivo*) in a 5% sucrose solution was injected

directly into the tumor. Such intervention was performed half-weekly. The siRNA sequences used for injections into the xenograft tumors are listed in the following table.

| Gene name | Sense (5′–3′) | Antisense (5′–3′) |
|---|---|---|
| HNRNPC | GCCUUCGUUCAGUAUGUUAAT-dTdTdTdTdTdTdT | AUUAACAUACUGAACGAAGGC-dAdAdAdAdAdAdA |
| LMNA | GAAGCAACUUCAGGAUGAGAU-dTdTdTdTdTdTdT | AUCUCAUCCUGAAGUUGCUUC-dAdAdAdAdAdAdA |
| NC | UUCUCCGAACGUGUCACGU-dTdTdTdTdTdTdT | ACGUGACACGUUCGGAGAAdA-dAdAdAdAdAdAdA |

The tumor volumes were measured, weekly or half-weekly, with a digital vernier caliper and calculated using the formula (long dimension/2) × (short dimension)$^2$. Finally, the mice were sacrificed, and the tumors were isolated, photographed, and weighed. To confirm gene knock-down in the grown tumors, small fractions of the tumors were also collected for RNA extraction and qPCR assays.

## Quantitative real-time PCR

Approximately 100,000 cells were harvested and lysed in 50 μl cell lysis buffer (Ambion). Cell lysate were subjected to DNase I treatment (Invitrogen) following the manufacturer's protocol. cDNA was synthesized using High-Capacity cDNA Reverse Transcription Kit (Invitrogen). cDNA was diluted 1:5 in nuclease-free water and used as templates for quantitative PCR, which was carried out in 25 μl volume using SYBR Green Master Mix (Invitrogen) with 4 μM each PCR primer on the VIIA7 system (Applied Biosystems). Primer sequences are listed in the following table.

| Gene name | Forward primer (5′–3′) | Reverse primer (5′–3′) |
|---|---|---|
| Beta-actin | CTGCCCTGAGGCACTCTT | TGTTGGCGTACAGGTCTTTG |
| HNRNPC | GCCAGCAACGTTACCAACAA | TGAACAGAGCAGCCCACAAT |
| IFNB1 | AACTGCAACCTTTCGAAGCC | AGAAGCACAACAGGAGAGCA |
| IFI27 | TGGCCAGGATTGCTACAGTTG | TATGGAGGACGAGGCGATTC |
| IFI44 | GTGAGGTCTGTTTTCCAAGGGC | CGGCAGGTATTTGCCATCTTTCC |
| IFI44L | TGCACTGAGGCAGATGCTGCG | TCATTGCGGCACACCAGTACAG |
| IRF1 | GAGGAGGTGAAAGACCAGAGCA | TAGCATCTCGGCTGGACTTCGA |
| IRF7 | CCACGCTATACCATCTACCTGG | GCTGCTATCCAGGGAAGACACA |
| IFIH1 | GCTGAAGTAGGAGTCAAAGCCC | CCACTGTGGTAGCGATAAGCAG |
| DDX58 | CACCTCAGTTGCTGATGAAGGC | GTCAGAAGGAAGCACTTGCTACC |
| MAVS | ATGGTGCTCACCAAGGTGTCTG | TCTCAGAGCTGCTGTCTAGCCA |
| PKR | GAAGTGGACCTCTACGCTTTGG | TGATGCCATCCCGTAGGTCTGT |
| PPIB | AACGCAGGCAAAGACACCAACG | TCTGTCTTGGTGCTCTCCACCT |

| Gene name | Forward primer (5′–3′) | Reverse primer (5′–3′) |
|---|---|---|
| LMNA | ATGAGGACCAGGTGGAGCAGTA | ACCAGGTTGCTGTTCCTCTCAG |
| STAU1 | AGAAGGAGCCAGAGTACACGCT | ATGTTCTCGGCTGCATTGCGCT |
| STAU2 | GAGTGGTCCAAAGCCTGGGTTT | CCAGAGATTACTTTGTGGCGGC |
| UPF1 | AACGAGCACCAAGGCATTGGCT | GGCTGCTTTGATAGTGCCTTCG |
| SMG6 | GATGGTCTTGCCATTCGCAGCA | TCGCTGTATCACTGGCTTGCTC |
| OAS1 | CCCTCTTTTCCCACCTCGTCAA | CACAGGTTCCTTGGACTCTGGT |
| OAS2 | GCTTCCGACAATCAACAGCCAAG | CTTGACGATTTTGTGCCGCTCG |
| OAS3 | CACCAAACCAAATCCCCAGG | TTTCCTTTGTTCTGAGCCGC |
| IFIT1 | GCCTTGCTGAAGTGTGGAGGAA | ATCCAGGCGATAGGCAGAGATC |
| IFIT2 | GGAGCAGATTCTGAGGCTTTGC | GGATGAGGCTTCCAGACTCCAA |
| IFIT3 | CCTGGAATGCTTACGGCAAGCT | GAGCATCTGAGAGTCTGCCCAA |
| IFIT5 | CGTCCTTCGTTATGCAGCCAAG | CCCTGTAGCAAAGTCCCATCTG |
| ADAR1 | TCCGTCTCCTGTCCAAAGAAGG | TTCTTGCTGGGAGCACTCACAC |

## Western blot

Cells were collected and lysed in RIPR buffer (Beyotime) supplemented with the protease inhibitor cocktail (Roche). Protein concentrations were quantified using the BCA protein assay (Pierce). The cell lysate containing 30 μg total protein was heat-denatured and subjected to SDS–PAGE, followed by transferring to PVDF membrane. The membrane was incubated with the primary and secondary antibodies and visualized with SuperSignal West Pico Chemiluminescent HRP substrate (Thermo). The anti-HNRNPC, anti-PKR, anti-beta-actin, and anti-alpha-tubulin antibodies were purchased from Abcam. Nuclear and cytoplasmic fraction proteins were separated by Nuclear/Cytosol Fractionation Kit (Biovision, K266-25). The density quantifications were analyzed by ImageJ software.

## ELISA for quantification of IFNβ concentration in cell medium

MCF7 and T47D cells were seeded in 96-well plates at density of 10,000 cells per well. After siRNA or shRNA treatments, the cells were cultured in fresh media for 48 h. The culturing media were then collected and assayed for the concentration of IFNβ with the VeriKine-HS Human Interferon Beta Serum ELISA Kit (PBL Interferon Source 41415-1), following the manufacturer's protocol. The absorbance at 450mm was measured on a SpectraMax M5 plate reader. Different concentrations of the IFNβ standard were used to generate a standard curve, which was then used to infer the IFNβ concentrations in the cell media.

## Immunofluorescence staining

Coverslips in 24-well plates were pretreated with 50 μg/ml poly-D-lysine (Beyotime) before planting the cells. After 48 h of culturing, the cells were washed twice with PBS and fixed with cold methanol for 15 min. Before the immunostaining, the cells were again washed twice with PBS, incubated with 0.2% Triton (Sigma) for 30 min, and then blocked with 3% BSA for 1 h at room temperature. The coverslips were then incubated with primary antibody (SCICONS, clone J2; Abcam HNRNPC ab133607, DDX58 ab45428) overnight at 4°C, followed by washing and incubation with secondary antibody (Abcam, ab150105, ab150092) for 1 h at room temperature. The coverslips were stained with 1mg/ml DAPI (Sigma) for 5 min and washed three times for 5 min with TBST. Then cells were washed for 10 min with PBS. Next, cells were mounted on a slide with Prolong Gold Antifade Mountant (Thermo) and stored in a dark chamber. Analysis was performed with a Zeiss LSM 710 confocal microscope. The fluorescence density plots were generated with the ImageJ software for quantification of the green fluorescence intensities (IF of dsRNA) obtained by the confocal microscope. More than 100 areas for each condition were randomly selected for the quantification. The results were summarized as box plots. The values on the *y*-axis represent the gray density of dsRNA staining by fluorescence (artificial unit).

## Cloning of DDX58 mutants and rescue of DDX58 expression

Full-length cDNA of DDX58 was ordered from YOUBIO company. Wild-type DDX58, DDX58 with alanine substitution mutations in key lysine residues (K858 and K861), and DDX58 dCTD truncation (1–776 aa) were cloned to expression plasmid (pCDH-GFP$^+$Puro, from YOUBIO company). 12 h after siRNA transfection, forward transfection of wild-type and mutant DDX58 plasmids was performed to rescue the expression of DDX58. 48 h after transfection, cells were harvested for RT–qPCR.

## Total RNA sequencing

Cells were collected 48 h after siRNA transfection. The nuclear and cytoplasmic fractions were separated with Nuclear/Cytosol Fractionation Kit (Biovision, K266-25). Total RNAs were then extracted from the nuclear and cytoplasmic lysates, separately, with TRIzol Reagent (Invitrogen). The residual genome DNA was removed by TURBO DNase (Ambion), and ribosomal RNA was removed with the Ribo-Zero Kit for human (Epicentre). About 100ng ribosomal RNA-depleted cytoplasmic RNA was used for cDNA library preparation with TruSeq RNA sample Preparation Kit (Illumina).

## Differential expression analysis and gene set function annotation

TruSeq library 2 × 125 reads from total RNA sequencing were first pre-processed using Cutadapt to remove adaptors and trim low-quality bases from 5′ and/or 3′ ends. After discarding reads shorter than 20 bp, paired-end reads were mapped to hg38 genome using the splice-aware algorithm RSEM (v1.2.15; Li & Dewey, 2011) with GENCODE v23 (Harrow *et al*, 2012) reference annotation and the following parameters: "–bowtie2 –paired-end". For T47D TruSeq data, only read1 was used for gene differential analysis and gene function analysis. So the parameter "–paired-end" was not used.

Gene differential expression analyses were performed with the R package DESeq (Anders & Huber, 2010). The list of ISG genes marked on the volcano plots was obtained from literature (Schoggins *et al*, 2011). Significantly up-regulated (log2 fold change > 1.5 and *P*-value < 0.001 siHNRNPC vs. siNC) genes were used for gene set function annotation analysis with DAVID (Huang *et al*, 2007).

## Inference of the differentially activated transcription factors upon HNRNPC repression

The MARINa (Lim *et al*, 2009) was used to infer the transcription factors (TFs) that are differentially activated upon HNRNPC silencing. First, the ARACNe (Margolin *et al*, 2006; Rodriguez-Barrueco *et al*, 2015) was used to predict the target gene set for each TF. Specifically, we used the gene expression profiles of 726 breast cancer tumors in The Cancer Genome Atlas (TCGA), and the parameters of the algorithm were set as follows: *P*-value threshold, 10e-6; DPI tolerance, 0.15; and number of bootstraps, 100. Finally, 14,652 target genes were inferred for 1,458 TFs. Next, from the RNA sequencing data analysis as described above, all the genes were ranked by their differential expression upon silencing of HNRNPC, from the most up-regulated to the most down-regulated. For each TF, MARINa then assesses enrichment of the predicted targets in the differentially expressed genes. If the positively and negatively regulated target genes are enriched in the up- and down-regulated genes by HNRNPC knock-down, respectively, the corresponding TF is defined as a master TF, whose functional activity is up-regulated upon HNRNPC repression. Statistical significance of such enrichment was tested by comparing the enrichment score with those from the same analysis but after gene permutations for 10,000 times. TFs with FDR-corrected *P* < 0.01 were inferred as master regulators that drive the gene expression program shift in response to HNRNPC knock-down.

## Enrichment of the dsRNA by immunoprecipitation with anti-dsRNA J2 antibody

This assay was designated to enrich the dsRNA species from the small RNA fraction (< 500 nt) of the total RNA. First, about 50 million cells grown on culturing dishes were washed twice with cold PBS. The protocol of TRIzol Reagent (Ambion, 15596-018) was then used to get the aqueous phase containing the total RNA, which was subjected to further removal of contaminating DNA with the HiPure DNA Mini Column II (Magen, R5214). 1/3 volume 100% ethanol was added to the filtrate containing the purified RNA, which was then passed through the HiPure RNA Mini Column I (Magen, R5214). This precipitates the fraction of RNA roughly longer than 500 nt on the column (data not shown). The remaining small RNA fraction (< 500 nt) was then precipitated with 60% ethanol and purified with AllPure Cell Kit (Magen, R5214). 10% Urea-PAGE gel was used to assess the purity and size (< 500 nt) of the isolated RNA fraction.

Next, the purified and size-selected RNA was subjected to immunoprecipitation with the anti-dsRNA antibody J2 (SCICONS, clone J2). Specifically, 60 μg RNA from the siNC or siHNRNPC cells was added to 1 ml fresh prepared IP lysis buffer (Pierce, 87787), supplemented with 20 U/ml RNase inhibitor and 1× PMSF (Biyuntian). Pre-clearing of the unspecific binding was done by incubating the RNA in lysis buffer with 50 μl Dynabeads® Protein G (Thermo Fisher, 10004D) for 30 min at 4°C on a horizontal shaker. After

centrifugation (14,000 *g* at 4°C for 5 min), 200 ng RNA was taken from the supernatant and would be used as a reference sample as "input". The remaining supernatant was then equally divided into two parts, one for the anti-dsRNA antibody J2 and the other for the IgG control of the same isotype. 10 μg of J2 or IgG was added into the supernatant, followed by incubation overnight on a rotating shaker at 4°C. 40 μl of Dynabeads® Protein G was then added into each reaction, followed by incubation for another 3 h at 4°C with gentle rocking. Next, the beads were collected and washed with 800 μl pre-chilled washing buffer (TBS buffer) for 5 times. Finally, the co-precipitated RNA on the beads were purified with TRIzol Reagent and re-dissolved with 12 μl nuclease-free water.

### Identification of the dsRNA regions from the dsRNA libraries

For the cells of siNC and siHNRNPC, the RNA samples immunoprecipitated with the anti-dsRNA J2, IgG, or the input RNA were used for preparation of the sequencing libraries. The small RNA sequencing library preparation kit, NEBNext Multiplex Small RNA Library Prep Set for Illumina (New England Biolabs, E7580S), was used, followed by high-throughput sequencing on a Illumina X10 platform with the 150 bp paired-end reading strategy.

The full-length gene sequences from GENCODE version 23 reference annotation (GRCh38) were used to build bowtie2 indices. The sequencing reads from the dsRNA libraries were pre-processed using Cutadapt to remove the adaptors and trim the low-quality bases from 5′ and/or 3′ ends. The reads shorter than 20 bp were discarded, and among the remaining reads, the rRNA- and tRNA-derived reads were also removed. Next, to facilitate direct and fair comparison between the dsRNA sequencing reads from different samples, we down-sampled each library to the same number of pre-processed and filtered reads. The reads were then mapped to the full-length transcriptome sequences from GENCODE version 23 reference annotation (GRCh38) in a forward strand-specific manner, with the default alignment strategy (bowtie2 –end-to-end –norc –k20), which allows up to 20 best alignments being reported. For each gene, the best aligned reads were collected and re-mapped onto the reverse strand of the same particular gene, with relatively loose restrictions and all alignments reported (bowtie2 –local –nofw -a -D 20 -R 3 -N 0 -L 10 -i S,1,0.50 –score-min G,10,2). Next, the overlapping alignments from the forward or reverse strand were merged, with the bedtools "intersect" (Quinlan, 2014). These regions, after removal of the duplicates and filtering by length (at least 15 nt), were treated as candidate dsRNA regions. Last, the dsRNA-enriched library reads were re-mapped onto these candidate dsRNA regions with local mode (bowtie2 –local –L 15 –norc –k20), and only the regions with at least two supporting reads were finally identified as dsRNA regions. The dsRNA enrichment and identification pipeline were performed with two biological replicates. The numbers of dsRNA regions identified in both replicates were provided in Fig 6B.

### 5′-Triphosphate RNA sequencing

5′-Triphosphate RNA sequencing assays were performed with a similar methodology as previously described (Nabet *et al*, 2017). To enrich for 5′-triphosphate RNA, 100–200 μg of small RNA or RNA from J2 IP was treated by Xrn-1 (NEB), which removes 5′-monophosphate RNA. Next, 5′ppp ends were converted to 5′p with RppH (NEB) in NEBuffer 2 (NEB). This allows ligation of RNA adaptor P5_RNA to the RNAs that originally have 5′-triphosphate. Finally, small RNA sequencing library preparation procedure was followed to generate the sequencing library for the RNA species with 5′ppp.

### Quantitative comparisons of the dsRNA libraries

Union of the dsRNA regions identified in the two dsRNA libraries, from the siHNRNPC and siNC cells, was used for quantifications of the dsRNA species in different samples. Specifically, the sequencing reads from the dsRNA libraries were mapped to the dsRNA regions with local mode (bowtie2 –local –L 15 –norc –k20). Only the best alignments for each read were selected, and the read count for each region in a sample was used as a quantification for the abundance of the particular dsRNA region. With these data, we made an MA plot to show the overall difference in the dsRNA regions by comparing their read counts in siHNRNPC and siNC cells. 928 up-regulated dsRNA regions were identified from the MA plot, which exhibited markedly higher read counts in siHNRNPC cells.

Frequencies of the Alu repeat sequences in these 928 up-regulated dsRNA regions were assessed with RepeatMasker (version open 4.0.6). For the purpose of comparison, the same number of intra-genic regions with the same length distribution as the 928 up-regulated dsRNA regions was randomly selected with the bedtools "shuffle". Such process was performed for 10 times, generating 10 random sets of intra-genic regions, which were also assessed by RepeatMasker for the percentages of regions that have Alu.

### Analysis of the dsRNA-originating introns

Annotations of introns were extracted from the GENCODE v23 reference annotation with a customized Perl script. Specifically, for multi-transcript genes, an intron was defined as any transcriptome region that is annotated as intron, by the reference genome, in at least one transcript from a gene. Next, the dexseq_prepare_annotation.py script from DEXseq package (Anders *et al*, 2012) was used to collapse the overlapping introns from multiple transcripts.

The HNRNPC binding region information was derived from Zarnack *et al* (2013) and downloaded from starBase v2.0 (Guo *et al*, 2014). 698 introns were found to harbor 864 of 928 up-regulated dsRNA regions shown in Fig 6C, and the percentages of these introns that have at least one of the HNRNPC binding regions were counted to generate Fig 6E. For comparison, out of all the introns genome-wide, 10 sets of randomly selected 698 introns with the same length distribution as the dsRNA-hosting introns were generated, and the percentages of these 10 sets that have the HNRNPC binding regions were counted, for the box plot in Fig 6E.

## Data availability

The gene expression data sets generated in this study are available in the GEO database repository (https://www.ncbi.nlm.nih.gov/geo/, GEO accession ID: GSE100451).

**Expanded View** for this article is available online.

## Acknowledgements

## Author contributions

YWu, WZ, and XY conceived and designed the experiments. YL and YWu conducted the bioinformatics analysis of the data, with help from ZX, HX, and YWa. YWu and WZ performed all the experiments. QZ helped the RNA-seq experiments. XL and XT helped the shRNA- and sgRNA-mediated gene knockdown. XY supervised the whole project. YWu, WZ, YL, and XY wrote the manuscript. All authors have read and approved the final manuscript.

## Conflict of interest

The authors declare that they have no conflict of interest.

# References

Anantha RW, Alcivar AL, Ma JL, Cai H, Simhadri S, Ule J, Konig J, Xia B (2013) Requirement of heterogeneous nuclear ribonucleoprotein C for BRCA gene expression and homologous recombination. *PLoS One* 8: e61368

Anders S, Huber W (2010) Differential expression analysis for sequence count data. *Genome Biol* 11: R106

Anders S, Reyes A, Huber W (2012) Detecting differential usage of exons from RNA-seq data. *Genome Res* 22: 2008–2017

Attig J, Ruiz de Los Mozos I, Haberman N, Wang Z, Emmett W, Zarnack K, Konig J, Ule J (2016) Splicing repression allows the gradual emergence of new Alu-exons in primate evolution. *Elife* 5: e19545

Baum A, Sachidanandam R, Garcia-Sastre A (2010) Preference of RIG-I for short viral RNA molecules in infected cells revealed by next-generation sequencing. *Proc Natl Acad Sci USA* 107: 16303–16308

Boelens MC, Wu TJ, Nabet BY, Xu B, Qiu Y, Yoon T, Azzam DJ, Twyman-Saint Victor C, Wiemann BZ, Ishwaran H, Ter Brugge PJ, Jonkers J, Slingerland J, Minn AJ (2014) Exosome transfer from stromal to breast cancer cells regulates therapy resistance pathways. *Cell* 159: 499–513

Chen Q, Gong B, Mahmoud-Ahmed AS, Zhou A, Hsi ED, Hussein M, Almasan A (2001) Apo2L/TRAIL and Bcl-2-related proteins regulate type I interferon-induced apoptosis in multiple myeloma. *Blood* 98: 2183–2192

Chiappinelli KB, Strissel PL, Desrichard A, Li H, Henke C, Akman B, Hein A, Rote NS, Cope LM, Snyder A, Makarov V, Budhu S, Slamon DJ, Wolchok JD, Pardoll DM, Beckmann MW, Zahnow CA, Merghoub T, Chan TA, Baylin SB *et al* (2015) Inhibiting DNA Methylation causes an interferon response in cancer via dsRNA including endogenous retroviruses. *Cell* 162: 974–986

Christian KJ, Lang MA, Raffalli-Mathieu F (2008) Interaction of heterogeneous nuclear ribonucleoprotein C1/C2 with a novel cis-regulatory element within p53 mRNA as a response to cytostatic drug treatment. *Mol Pharmacol* 73: 1558–1567

Chung H, Calis JJA, Wu X, Sun T, Yu Y, Sarbanes SL, Dao Thi VL, Shilvock AR, Hoffmann HH, Rosenberg BR, Rice CM (2018) Human ADAR1 prevents endogenous RNA from triggering translational shutdown. *Cell* 172(811–824): e14

Deininger P (2011) Alu elements: know the SINEs. *Genome Biol* 12: 236

DeWitte-Orr SJ, Mossman KL (2010) dsRNA and the innate antiviral immune response. *Future Virol* 5: 325–341

Eberle AB, Lykke-Andersen S, Muhlemann O, Jensen TH (2009) SMG6 promotes endonucleolytic cleavage of nonsense mRNA in human cells. *Nat Struct Mol Biol* 16: 49–55

Goel S, DeCristo MJ, Watt AC, BrinJones H, Sceneay J, Li BB, Khan N, Ubellacker JM, Xie S, Metzger-Filho O, Hoog J, Ellis MJ, Ma CX, Ramm S, Krop IE, Winer EP, Roberts TM, Kim HJ, McAllister SS, Zhao JJ (2017) CDK4/6 inhibition triggers anti-tumour immunity. *Nature* 548: 471–475

Goubau D, Deddouche S, Reis e Sousa C (2013) Cytosolic sensing of viruses. *Immunity* 38: 855–869

Goubau D, Schlee M, Deddouche S, Pruijssers AJ, Zillinger T, Goldeck M, Schuberth C, Van der Veen AG, Fujimura T, Rehwinkel J, Iskarpatyoti JA, Barchet W, Ludwig J, Dermody TS, Hartmann G, Reis e Sousa C (2014) Antiviral immunity via RIG-I-mediated recognition of RNA bearing 5′-diphosphates. *Nature* 514: 372–375

Gruber AJ, Schmidt R, Gruber AR, Martin G, Ghosh S, Belmadani M, Keller W, Zavolan M (2016) A comprehensive analysis of 3′ end sequencing data sets reveals novel polyadenylation signals and the repressive role of heterogeneous ribonucleoprotein C on cleavage and polyadenylation. *Genome Res* 26: 1145–1159

Guo S, Tan L, Pu W, Wu J, Xu K, Wu J, Li Q, Ma Y, Xu J, Jin L, Wang J (2014) Quantitative assessment of the diagnostic role of APC promoter methylation in non-small cell lung cancer. *Clin Epigenetics* 6: 5

Harrow J, Frankish A, Gonzalez JM, Tapanari E, Diekhans M, Kokocinski F, Aken BL, Barrell D, Zadissa A, Searle S, Barnes I, Bignell A, Boychenko V, Hunt T, Kay M, Mukherjee G, Rajan J, Despacio-Reyes G, Saunders G, Steward C *et al* (2012) GENCODE: the reference human genome annotation for The ENCODE Project. *Genome Res* 22: 1760–1774

Hasler J, Samuelsson T, Strub K (2007) Useful 'junk': Alu RNAs in the human transcriptome. *Cell Mol Life Sci* 64: 1793–1800

Holcik M, Gordon BW, Korneluk RG (2003) The internal ribosome entry site-mediated translation of antiapoptotic protein XIAP is modulated by the heterogeneous nuclear ribonucleoproteins C1 and C2. *Mol Cell Biol* 23: 280–288

Honda K, Takaoka A, Taniguchi T (2006) Type I interferon [corrected] gene induction by the interferon regulatory factor family of transcription factors. *Immunity* 25: 349–360

Huang DW, Sherman BT, Tan Q, Collins JR, Alvord WG, Roayaei J, Stephens R, Baseler MW, Lane HC, Lempicki RA (2007) The DAVID gene functional classification tool: a novel biological module-centric algorithm to functionally analyze large gene lists. *Genome Biol* 8: R183

Hug N, Longman D, Caceres JF (2016) Mechanism and regulation of the nonsense-mediated decay pathway. *Nucleic Acids Res* 44: 1483–1495

Ivashkiv LB, Donlin LT (2014) Regulation of type I interferon responses. *Nat Rev Immunol* 14: 36–49

Kaneko H, Dridi S, Tarallo V, Gelfand BD, Fowler BJ, Cho WG, Kleinman ME, Ponicsan SL, Hauswirth WW, Chiodo VA, Kariko K, Yoo JW, Lee DK, Hadziahmetovic M, Song Y, Misra S, Chaudhuri G, Buaas FW, Braun RE, Hinton DR *et al* (2011) DICER1 deficit induces Alu RNA toxicity in age-related macular degeneration. *Nature* 471: 325–330

Kawai T, Akira S (2008) Toll-like receptor and RIG-I-like receptor signaling. *Ann N Y Acad Sci* 1143: 1–20

Kim JH, Paek KY, Choi K, Kim TD, Hahm B, Kim KT, Jang SK (2003) Heterogeneous nuclear ribonucleoprotein C modulates translation of c-myc mRNA in a cell cycle phase-dependent manner. *Mol Cell Biol* 23: 708−720

Kim YK, Furic L, Desgroseillers L, Maquat LE (2005) Mammalian Staufen1 recruits Upf1 to specific mRNA 3′UTRs so as to elicit mRNA decay. *Cell* 120: 195−208

Kim YK, Furic L, Parisien M, Major F, DesGroseillers L, Maquat LE (2007) Staufen1 regulates diverse classes of mammalian transcripts. *EMBO J* 26: 2670−2681

Konig J, Zarnack K, Rot G, Curk T, Kayikci M, Zupan B, Turner DJ, Luscombe NM, Ule J (2010) iCLIP reveals the function of hnRNP particles in splicing at individual nucleotide resolution. *Nat Struct Mol Biol* 17: 909−915

Kurosaki T, Maquat LE (2016) Nonsense-mediated mRNA decay in humans at a glance. *J Cell Sci* 129: 461−467

Lee EK, Kim HH, Kuwano Y, Abdelmohsen K, Srikantan S, Subaran SS, Gleichmann M, Mughal MR, Martindale JL, Yang X, Worley PF, Mattson MP, Gorospe M (2010) hnRNP C promotes APP translation by competing with FMRP for APP mRNA recruitment to P bodies. *Nat Struct Mol Biol* 17: 732−739

Leonova KI, Brodsky L, Lipchick B, Pal M, Novototskaya L, Chenchik AA, Sen GC, Komarova EA, Gudkov AV (2013) p53 cooperates with DNA methylation and a suicidal interferon response to maintain epigenetic silencing of repeats and noncoding RNAs. *Proc Natl Acad Sci USA* 110: E89−E98

Li B, Dewey CN (2011) RSEM: accurate transcript quantification from RNA-Seq data with or without a reference genome. *BMC Bioinformatics* 12: 323

Liddicoat BJ (2015) RNA editing by ADAR1 prevents MDA5 sensing of endogenous dsRNA as nonself. *Science* 349: 1115−1120

Lim WK, Lyashenko E, Califano A (2009) Master regulators used as breast cancer metastasis classifier. *Pac Symp Biocomput* 2009: 504−515

Lopez de Padilla CM, Niewold TB (2016) The type I interferons: basic concepts and clinical relevance in immune-mediated inflammatory diseases. *Gene* 576: 14−21

Maeda S, Wada H, Naito Y, Nagano H, Simmons S, Kagawa Y, Naito A, Kikuta J, Ishii T, Tomimaru Y, Hama N, Kawamoto K, Kobayashi S, Eguchi H, Umeshita K, Ishii H, Doki Y, Mori M, Ishii M (2014) Interferon-alpha acts on the S/G2/M phases to induce apoptosis in the G1 phase of an IFNAR2-expressing hepatocellular carcinoma cell line. *J Biol Chem* 289: 23786−23795

Mannion NM, Greenwood SM, Young R, Cox S, Brindle J, Read D, Nellaker C, Vesely C, Ponting CP, McLaughlin PJ, Jantsch MF, Dorin J, Adams IR, Scadden AD, Ohman M, Keegan LP, O'Connell MA (2014) The RNA-editing enzyme ADAR1 controls innate immune responses to RNA. *Cell Rep* 9: 1482−1494

Margolin AA, Wang K, Lim WK, Kustagi M, Nemenman I, Califano A (2006) Reverse engineering cellular networks. *Nat Protoc* 1: 662−671

McCloskey A, Taniguchi I, Shinmyozu K, Ohno M (2012) hnRNP C tetramer measures RNA length to classify RNA polymerase II transcripts for export. *Science* 335: 1643−1646

McNab F, Mayer-Barber K, Sher A, Wack A, O'Garra A (2015) Type I interferons in infectious disease. *Nat Rev Immunol* 15: 87−103

Meng Z, Jackson NL, Choi H, King PH, Emanuel PD, Blume SW (2008) Alterations in RNA-binding activities of IRES-regulatory proteins as a mechanism for physiological variability and pathological dysregulation of IGF-IR translational control in human breast tumor cells. *J Cell Physiol* 217: 172−183

Moretti JE, Muller UF (2014) A ribozyme that triphosphorylates RNA 5′-hydroxyl groups. *Nucleic Acids Res* 42: 4767−4778

Mulnix RE, Pitman RT, Retzer A, Bertram C, Arasi K, Crees Z, Girard J, Uppada SB, Stone AL, Puri N (2014) hnRNP C1/C2 and Pur-beta proteins mediate induction of senescence by oligonucleotides homologous to the telomere overhang. *Onco Targets Ther* 7: 23−32

Murata M, Nabeshima S, Kikuchi K, Yamaji K, Furusyo N, Hayashi J (2006) A comparison of the antitumor effects of interferon-alpha and beta on human hepatocellular carcinoma cell lines. *Cytokine* 33: 121−128

Nabet BY, Qiu Y, Shabason JE, Wu TJ, Yoon T, Kim BC, Benci JL, DeMichele AM, Tchou J, Marcotrigiano J, Minn AJ (2017) Exosome RNA unshielding couples stromal activation to pattern recognition receptor signaling in cancer. *Cell* 170: 352−366.e13

Nagarajan UM (2011) Induction and function of IFN beta during viral and bacterial infection. *Crit Rev Immunol* 31: 459−474

Park YM, Hwang SJ, Masuda K, Choi KM, Jeong MR, Nam DH, Gorospe M, Kim HH (2012) Heterogeneous nuclear ribonucleoprotein C1/C2 controls the metastatic potential of glioblastoma by regulating PDCD4. *Mol Cell Biol* 32: 4237−4244

Peisley A, Jo MH, Lin C, Wu B, Orme-Johnson M, Walz T, Hohng S, Hur S (2012) Kinetic mechanism for viral dsRNA length discrimination by MDA5 filaments. *Proc Natl Acad Sci USA* 109: E3340−9

Pino I, Pio R, Toledo G, Zabalegui N, Vicent S, Rey N, Lozano MD, Torre W, Garcia-Foncillas J, Montuenga LM (2003) Altered patterns of expression of members of the heterogeneous ribonucleoprotein (hnRNP) family in lung cancer. *Lung Cancer* 41: 131−143

Platanias LC (2005) Mechanisms of type-I- and type-II-interferon-mediated signalling. *Nat Rev Immunol* 5: 375−386

Popp MW, Maquat LE (2014) The dharma of nonsense-mediated mRNA decay in mammalian cells. *Mol Cells* 37: 1−8

Quinlan AR (2014) BEDTools: the swiss-army tool for genome feature analysis. *Curr Protoc Bioinformatics* 47: 11.12.1−11.12.34

Reikine S, Nguyen JB, Modis Y (2014) Pattern recognition and signaling mechanisms of RIG-I and MDA5. *Front Immunol* 5: 342

Rodriguez-Barrueco R, Yu J, Saucedo-Cuevas LP, Olivan M, Llobet-Navas D, Putcha P, Castro V, Murga-Penas EM, Collazo-Lorduy A, Castillo-Martin M, Alvarez M, Cordon-Cardo C, Kalinsky K, Maurer M, Califano A, Silva JM (2015) Inhibition of the autocrine IL-6-JAK2-STAT3-calprotectin axis as targeted therapy for HR-/HER2+ breast cancers. *Genes Dev* 29: 1631−1648

Roers A, Hiller B, Hornung V (2016) Recognition of endogenous nucleic acids by the innate immune system. *Immunity* 44: 739−754

Roulois D, Loo Yau H, Singhania R, Wang Y, Danesh A, Shen SY, Han H, Liang G, Jones PA, Pugh TJ, O'Brien C, De Carvalho DD (2015) DNA-demethylating agents target colorectal cancer cells by inducing viral mimicry by endogenous transcripts. *Cell* 162: 961−973

Sanceau J, Hiscott J, Delattre O, Wietzerbin J (2000) IFN-beta induces serine phosphorylation of Stat-1 in Ewing's sarcoma cells and mediates apoptosis via induction of IRF-1 and activation of caspase-7. *Oncogene* 19: 3372−3383

Sangfelt O, Erickson S, Castro J, Heiden T, Einhorn S, Grander D (1997) Induction of apoptosis and inhibition of cell growth are independent responses to interferon-alpha in hematopoietic cell lines. *Cell Growth Differ* 8: 343−352

Schepens B, Tinton SA, Bruynooghe Y, Parthoens E, Haegman M, Beyaert R, Cornelis S (2007) A role for hnRNP C1/C2 and Unr in internal initiation of translation during mitosis. *EMBO J* 26: 158−169

Schlee M, Hartmann G (2016) Discriminating self from non-self in nucleic acid sensing. *Nat Rev Immunol* 16: 566−580

Schmidt SA, Foley PL, Jeong DH, Rymarquis LA, Doyle F, Tenenbaum SA, Belasco JG, Green PJ (2015) Identification of SMG6 cleavage sites and a preferred RNA cleavage motif by global analysis of endogenous NMD targets in human cells. *Nucleic Acids Res* 43: 309–323

Schneider WM, Chevillotte MD, Rice CM (2014) Interferon-stimulated genes: a complex web of host defenses. *Annu Rev Immunol* 32: 513–545

Schoggins JW, Wilson SJ, Panis M, Murphy MY, Jones CT, Bieniasz P, Rice CM (2011) A diverse range of gene products are effectors of the type I interferon antiviral response. *Nature* 472: 481–485

Schonborn J, Oberstrass J, Breyel E, Tittgen J, Schumacher J, Lukacs N (1991) Monoclonal antibodies to double-stranded RNA as probes of RNA structure in crude nucleic acid extracts. *Nucleic Acids Res* 19:2993–3000

Schreiber G, Piehler J (2015) The molecular basis for functional plasticity in type I interferon signaling. *Trends Immunol* 36: 139–149

Shetty S (2005) Regulation of urokinase receptor mRNA stability by hnRNP C in lung epithelial cells. *Mol Cell Biochem* 272: 107–118

Spahn A, Blondeau N, Heurteaux C, Dehghani F, Rami A (2008) Concomitant transitory up-regulation of X-linked inhibitor of apoptosis protein (XIAP) and the heterogeneous nuclear ribonucleoprotein C1-C2 in surviving cells during neuronal apoptosis. *Neurochem Res* 33: 1859–1868

Sun W, Xing B, Sun Y, Du X, Lu M, Hao C, Lu Z, Mi W, Wu S, Wei H, Gao X, Zhu Y, Jiang Y, Qian X, He F (2007) Proteome analysis of hepatocellular carcinoma by two-dimensional difference gel electrophoresis: novel protein markers in hepatocellular carcinoma tissues. *Mol Cell Proteomics* 6: 1798–1808

Sun Y, Han M, Kim C, Calvert JG, Yoo D (2012) Interplay between interferon-mediated innate immunity and porcine reproductive and respiratory syndrome virus. *Viruses* 4: 424–446

Svoboda P, Di Cara A (2006) Hairpin RNA: a secondary structure of primary importance. *Cell Mol Life Sci* 63: 901–908

Velusamy T, Shetty P, Bhandary YP, Liu MC, Shetty S (2008) Posttranscriptional regulation of urokinase receptor expression by heterogeneous nuclear ribonuclear protein C. *Biochemistry* 47: 6508–6517

Wang Y, Ludwig J, Schuberth C, Goldeck M, Schlee M, Li H, Juranek S, Sheng G, Micura R, Tuschl T *et al* (2010) Structural and functional insights into 5′-ppp RNA pattern recognition by the innate immune receptor RIG-I. *Nat Struct Mol Biol* 17: 781–787

West AP, Khoury-Hanold W, Staron M, Tal MC, Pineda CM, Lang SM, Bestwick M, Duguay BA, Raimundo N, MacDuff DA, Kaech SM, Smiley JR, Means RE, Iwasaki A, Shadel GS (2015) Mitochondrial DNA stress primes the antiviral innate immune response. *Nature* 520: 553–557

White E, Schlackow M, Kamieniarz-Gdula K, Proudfoot NJ, Gullerova M (2014) Human nuclear Dicer restricts the deleterious accumulation of endogenous double-stranded RNA. *Nat Struct Mol Biol* 21: 552–559

Williamson DJ, Banik-Maiti S, DeGregori J, Ruley HE (2000) hnRNP C is required for postimplantation mouse development but Is dispensable for cell viability. *Mol Cell Biol* 20: 4094–4105

Wu B, Peisley A, Richards C, Yao H, Zeng XH, Lin C, Chu FX, Walz T, Hur S (2013) Structural basis for dsRNA recognition, filament formation, and antiviral signal activation by MDA5. *Cell* 152: 276–289

Wu J, Chen ZJ (2014) Innate immune sensing and signaling of cytosolic nucleic acids. *Annu Rev Immunol* 32: 461–488

Yang Y, Shaffer AL 3rd, Emre NC, Ceribelli M, Zhang M, Wright G, Xiao W, Powell J, Platig J, Kohlhammer H *et al* (2012) Exploiting synthetic lethality for the therapy of ABC diffuse large B cell lymphoma. *Cancer Cell* 21: 723–737

Yang F, Yi F, Han X, Du Q, Liang Z (2013) MALAT-1 interacts with hnRNP C in cell cycle regulation. *FEBS Lett* 587: 3175–3181

Zarnack K, Konig J, Tajnik M, Martincorena I, Eustermann S, Stevant I, Reyes A, Anders S, Luscombe NM, Ule J (2013) Direct competition between hnRNP C and U2AF65 protects the transcriptome from the exonization of Alu elements. *Cell* 152: 453–466